Practical aspects on how to deracemize atropizomers by means of crystallization

Ryusei Oketani

Normandie Université

THÈSE

Pour obtenir le diplôme de doctorat

Spécialité Chimie

Préparée au sein de l'Université de Rouen Normandie

Practical aspects on how to deracemize atropisomers by means of crystallization

(Aspects pratiques de la déracémisation d'atropisomères par cristallisation)

Présentée et soutenue par
Ryusei OKETANI

Thèse soutenue publiquement le 06 Décembre 2019 devant le jury composé de		
M. Alexander BREDIKHIN	Pr FRC Kazan Scientific Center of RAS	Rapporteur
M. Joop Ter HORST	Pr University of Strathclyde	Rapporteur
M. Gérard COQUEREL	Pr Université de Rouen Normandie	Président
Mme. Sylvie FERLAY-CHARITAT	Pr Université de Strasbourg	Examinateur
M. Pascal CARDINAEL	Pr Université de Rouen Normandie	Directeur de thèse

Thèse dirigée par Pascal CARDINAEL professeur des universités et Co-encadrée par le Dr. Clément BRANDEL au laboratoire Sciences et Méthodes Séparatives (EA3233 SMS)

UNIVERSITÉ DE ROUEN NORMANDIE

ED 508 NC Normande de Chimie

SMS Sciences et Méthodes Séparatives

Acknowledgements

I would like to thank the members of the PhD commission for evaluating my work; Prof. Alexander Bredikhin and Prof. Joop Ter Horst for reviewing my manuscript and Prof. Gérard Coquerel and Prof. Sylvie Ferlay-Charitat for examining it.

My deepest appreciation goes to the head of SMS laboratory Prof. Gérard Coquerel and my supervisor Prof. Pascal Cardinael whose comments, suggestions and help were of inestimable value for my study and my living in France.

I am also immensely indebted to Dr. Clément Brandel who gave me invaluable comments and warm encouragements.

I shall be profoundly grateful to Prof. Hirohito Tsue who supervised me in my master and Prof. Rui Tamura in Kyoto University who gave me a chance to study in the group of Prof. Gérard Coquerel.

I wish to thank Dr. Hiroki Takahashi in Kyoto University for meaningful discussions and comments on my study.

I gratefully acknowledge past and present members of SMS laboratory, especially, Dr. Simon Clevers, Dr. Mélanie Mignot, Dr. Benjamin Schammé who took care of the start-up of my life in France.

I would also like to thank to CORE ITN project from the Horizon 2020 Research and Innovation Programme of the European Union under Marie Sklodowska-Curie Action, and Yoshida Scholarship Foundation for providing financial support to the project .

Finally, I would also like to express my gratitude to my wife Saori for her moral support and warm encouragements.

桶谷龍成

Contents

Abbreviations

DBU	1,8-diazabicyclo[5.4.0]undec-7-ene
DSC	Differential scanning calorimetry
ee	Enantiomeric excess
EtOAc	Ethyl acetate
EtOH	Ethanol
HPLC	High-performance liquid chromatography
iPrCN	Isobutyronitrile
IUPAC	International Union of Pure and Applied Chemistry
MeOH	Methanol
MIBK	Methyl isobutyl ketone
MTBE	Methyl tert-butyl ether
NMPA	*N*-(2-methylbenzylidene)phenylglycine amide
PC	Preferential crystallization
SC-XRD	Single-crystal X-ray diffraction
SOAT	Second-order asymmetric transformation
tBuOH	Tert-butyl alcohol
TCID	Temperature cycle-induced deracemization
THF	Tetrahydrofuran
VR	Viedma Ripening
XRPD	Powder X-ray diffraction

General introduction & Outline of the thesis

Chirality or asymmetry is a fundamental property and is of great importance in many natural systems, particularly in biology and pharmaceuticals. Indeed, the human body consists of a large variety of chiral amino acids and sugar molecules, and the availability of chiral separation techniques is paramount for enabling studies relating to the biological functions and activities of chiral molecules. Access to the desired polymorph and enantiomer of a particular compound is critical in the field of pharmaceutical chemistry owing to the differences in bioavailability and bioactivity among polymorphs and enantiomers. Among the 42 chemical drug entities approved by the Food and Drug Administration (FDA) in 2018, 25 molecules contain chiral centers,[1,2] and over 80% of the active pharmaceutical ingredients exhibit polymorphism or solvate formation,[3,4]. Additionally, their physical properties may vary, which makes chiral separation and polymorph control vital in drug development. Classic chiral resolution techniques, such as chemical transformation-mediated diastereomeric resolutions, are robust and reliable approaches to preparing enantiomerically pure materials and are preferentially used in industrial chemistry. However, in such approaches, the undesired enantiomer, which constitutes half of the product, is wasted. To reduce such waste and improve productivity, chiral separations by deracemization, an approach that combines racemization with crystallization, have been the subject of intense studies.

Viedma ripening (VR)[5–10] and temperature cycle-induced deracemization (TCID)[11–13] are major approaches by which to achieve deracemization and are being actively studied. We reported that a second-order asymmetric transformation (SOAT), which is a combination of stereoselective crystallization and racemization, could achieve a relatively high process productivity compared to TCID due to its short process time.[14]

Numerous examples of the deracemization of chiral crystals have been reported to date; however, further investigations are required for industrial applications because the optimization of the processes relies on empirical studies conducted on a case-by-case basis. In this context, the Marie Skłodowska-Curie Innovative Training Network on Continuous Resolution and Deracemization of

Chiral Compounds by Crystallization (CORE ITN) launched in 2016. The research objective of the CORE ITN is to construct an industrial toolbox with a continuous resolution that provides next-generation tools, approaches and methods to industry for the development of separation and purification processes (resolution). This thesis is in the framework of the CORE ITN and aims to provide guidelines for the optimization and design of deracemization processes for industrial applications by demonstrating experimental approaches.

In Chapter 2, we report the first experimental proof of the impact of racemization kinetics on global TCID kinetics as well as on process productivity. We chose an atropisomeric naphthamide derivative that can be racemized in a simple manner as a model compound to simplify the racemization kinetics. Indeed, the racemization kinetics are well described by first-order reaction kinetics and are linearly related to the global TCID kinetics. Interestingly, we found that the process productivity was related not only to the racemization kinetics but also to the solubility of the compound in the chosen solvent.

In Chapter 3, despite the operational simplicity of TCID, we noticed that its process productivity was quite low, and we conducted a comparison study of process productivities of TCID and SOAT using the same molecule and solvent. First, we clarified that the process productivity of TCID is essentially independent of the scale of the system. Then, we compared the productivities of the two process and found that although SOAT is a productive process, an additional operation (i.e. seeding) similar to preferential crystallization is required.

In Chapter 4, based on a thorough phase diagram study, we report a challenging and problematic case of the deracemization of a single compound to form multiple solid phases. In such a system, the phase diagram is useful for optimizing the crystallization pathway because it provides the landscape of the solid-liquid equilibrium. Indeed, even if many experimental cases of phase diagram-based chiral resolutions have been reported, the application of a phase diagram study in the context of deracemization has not yet been reported. Racemization adds complexity to the phase diagram and may cause confusion. Hence, we sought to show the construction of a phase diagram for racemizable compounds and how the diagram can be applied in deracemization in Chapter 4.

1. State of the Art

1.1 Chirality

Symmetry is associated with harmony and beautiful proportions in many cultures and exists everywhere in our universe. This ubiquitous property has attracted human interest since ancient times; for example, mirror symmetry is often found in ancient Greek architecture. On the other hand, an object that is nonsuperimposable on its mirror image, such as our two *hands*, is referred to as *"chiral"* (Figure 1.1). This word is derived from the ancient Greek word "χειρ (kheir)," meaning "hand." Although *"chirality"* is as abundant as is symmetry in the universe, it was recognized only recently by humans. In the field of chemistry, in 1815, Jean-Baptiste Biot discovered that polarized light could be rotated clockwise or counterclockwise when passing through a solution of an organic substance depending upon the optical axis of the material.[15] In 1848, Louis Pasteur discovered that sodium ammonium tetrahydrate salts of tartaric acid crystallize in mirror symmetrical shapes and that the crystals could be manually sorted based on their handedness.[16] This was the first chiral resolution reported. Once separated, he observed that a solution made from crystals of the same handedness rotated polarized light clockwise, while a solution made from crystals of the opposite handedness rotated light counterclockwise. This phenomenon arises from a feature of chiral molecules called "enantiomerism". It is now understood that this chiral separation of tartaric acid can only be reproduced below 27 °C, and the crystal structure was reported by Reiko Kuroda in 1981.[17] The purity of a mixture of enantiomers can be described by the enantiomeric excess (*ee*), which is defined as $|F_{(+)} - F_{(-)}|$, with the composition given as the mole or weight fractions $F_{(+)}$ and $F_{(-)}$ where $F_{(+)} + F_{(-)} = 1$.[18] A mixture of equal amounts of both enantiomers (*ee* = 0) is referred to as a racemate or racemate.

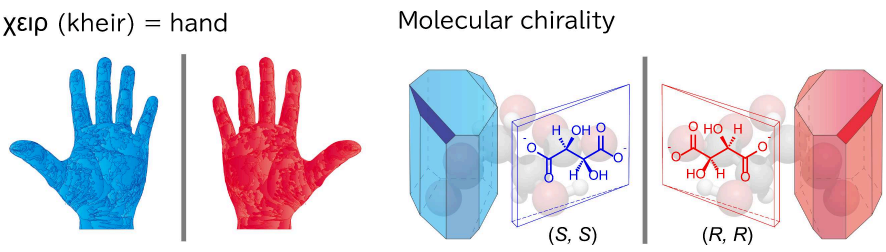

Figure 1.1 Schematic representation of the various types of chirality.

1.2 Chiral species in the crystalline state and their thermodynamic equilibria

Crystals are solid materials that have an essentially sharp diffraction pattern, meaning that most of the intensity of the diffraction is concentrated in relatively sharp Bragg peaks, occurring in addition to diffuse scattering.[19] The space group expresses the symmetric operations in the crystal structure, i.e., how the constituents are arranged in the crystal.[20] Although there are 230 space groups, only 65, known as the Sohncke groups, are compatible with chiral crystal structures (Table 1.1),[21] implying a limited number of available space groups for the crystallization of pure enantiomers.

Table 1.1 Sohncke groups.

System	Class	Space group
Triclinic	1	*P*1
Monoclinic	2	*P*2, $P2_1$, *C*2
Orthorhombic	222	*P*222, $P2_12_12_1$, $P2_12_12$, $P222_1$, *C*222, $C222_1$, *F*222, *I*222, $I2_12_12_1$
Tetragonal	4	*P*4, $P4_1$, $P4_2$, $P4_3$, *I*4, $I4_1$
	422	*P*422, $P42_12$, $P4_122$, $P4_12_12$, $P4_222$, $P4_22_12$, $P4_322$, *I*422, $I4_122$
Trigonal and Rhombohedral	3	*P*3, $P3_1$, $P3_2$, *R*3
	32	*P*312, *P*321, $P3_121$, $P3_112$, $P3_212$, $P3_221$, *R*32
Hexagonal	6	*P*6, $P6_5$, $P6_4$, $P6_3$, $P6_2$, $P6_1$
	622	*P*622, $P6_122$, $P6_222$, $P6_322$, $P6_422$, $P6_522$
Cubic	23	*P*23, *F*23, *I*23, $P2_13$, $I2_13$
	432	*P*432, $P4_122$, $P4_222$, $P4_322$, *P*432, $F4_132$, *I*432, $I4_132$

Three types of crystalline phases of racemates are: (i) the racemate forms a homogeneous solid phase with the two enantiomers present in equal amounts in each unit cell of the crystal lattice, (ii) the conglomerate is a 1:1 physical mixture of enantiopure crystals, and (iii) the total solid solution is a homogeneous solid solution containing equimolar amounts of the opposite enantiomers that are more or less unordered in the crystal (Figure 1.2).[22] In case of a conglomerate, a pair of enantiopure samples will crystallize either in the same space group containing only operations of the first kind (rotations, roto-translations, and translations) or in two enantiomorphic space groups when the structure involves mirror screw axes.[21] Racemic compounds can crystallize in any of the 230 space groups.

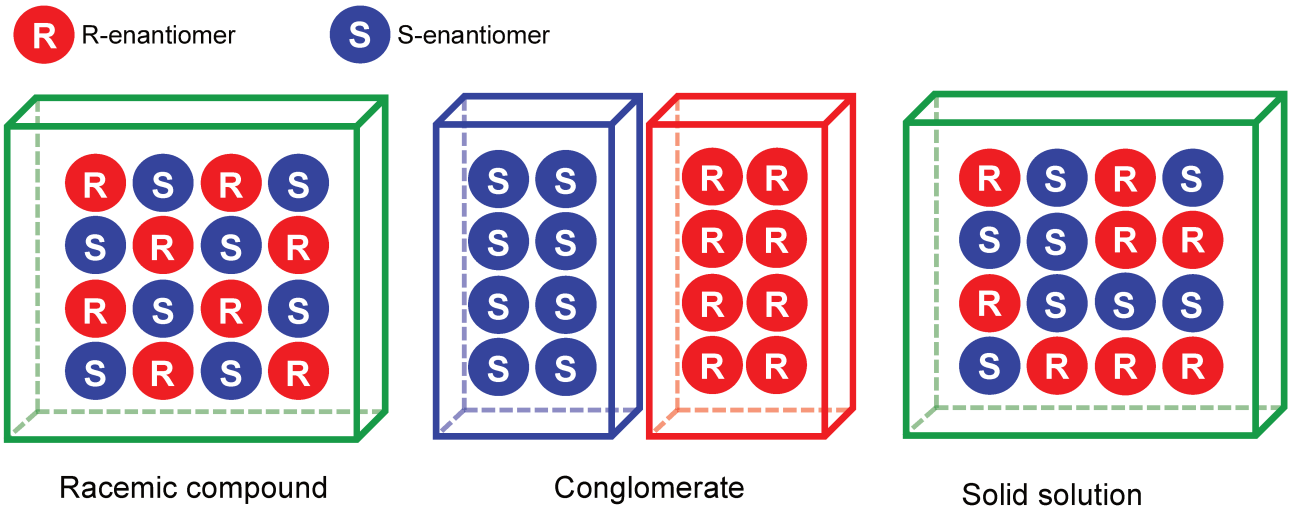

Figure 1.2 Schematic representation of the different types of chiral species in the crystalline state.

To understand the crystallization behavior of a mixture of enantiomers, a phase diagram must be established. A phase diagram is a graphical representation of the physical states of a substance in equilibrium.[22] It indicates not only the solubility of a component but also the amounts of which phases that are present at equilibrium, making it a valuable tool for the design of crystallization processes for mixtures of enantiomers. Figure 1.3 depicts the ternary isotherm systems corresponding to the three cases.

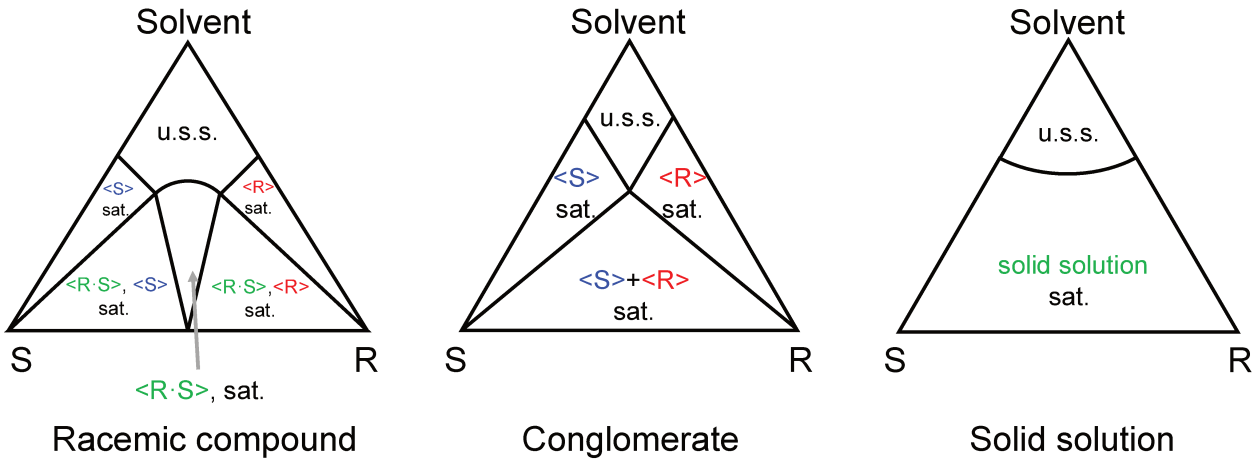

Figure 1.3 Three main possibilities of ternary phase diagrams of a pair of enantiomers and solvent. <R·S>: racemic compound, <R> and <S>: enantiopure crystal of the corresponding enantiomer, u.s.s.: undersaturated solution, sat.: saturated solution.

1.3 Chiral resolution

Homochirality in nature has vital implications for the activity of chiral substances in chiral environments, such as in biological systems. Chiral molecules in living organisms exist almost exclusively as single enantiomers, and many active pharmaceutical ingredients for medical purposes are used in their enantiomerically pure forms.[22] The notable case that highlighted the importance of enantiopure pharmaceuticals is the birth defect crisis caused by thalidomide in the 1960s. Later, studies discovered that while (*R*)-thalidomide has sedative effects, (*S*)-thalidomide is teratogenic and causes serious birth defects. Through this tragedy, it was confirmed that accesses to pure enantiomers is of paramount importance in understanding the biological activities of each enantiomer. Several routes for obtaining single enantiomers are listed below.

Stereoselective synthesis

- Catalysis
  - Organocatalysis[23]
  - Enzymes[24]
  - Coordination complexes[25–27]
  - Autocatalysis[28]
- Chiral auxiliary[29]
- Chiral pool (reagent)[30]

Resolution of racemates (without racemization)

- Chiral chromatography[31]
- Derivatization[32]
  - Diastereomer
  - Salt, Cocrystal
- Kinetic resolution[33]
- Direct enantio-convergent transformation[34]
- Crystallization
  - Preferential crystallization (PC)[35]
  - Preferential enrichment[36]

Resolution of racemates (with racemization)

- Dynamic kinetic resolution[37]
- Deracemization (Asymmetric transformation)
  - Viedma ripening (VR)[38]
  - Ostwald ripening[39]
  - Temperature cycle-induced deracemization (TCID)[40]
  - Second-order asymmetric transformation (SOAT)[41]

Stereoselective syntheses involve chemical reactions in which one or more new elements of chirality are formed in a substrate, producing stereoisomeric products in unequal amounts. In terms of sustainability, stereoselective synthesis is an excellent approach because accessing a single enantiomer is straightforward. However, for technical and practical reasons, the resolution of a racemate into pure enantiomers is often economically advantageous in industrial applications. For the sake of simplicity, in the present manuscript, the resolution techniques are categorized by whether or not racemization occurs during the process. The resolution techniques that do not involve racemization include "classical methods." Except for direct enantio-convergent transformations, all of these techniques consider the undesired enantiomers, *i.e.*, 50% of the product, as being an impurity. In contrast, a resolution combined with racemization can theoretically convert racemates into a single pure enantiomer with a 100% yield. Details of each technique and some examples are described in the listed references. The next section describes in detail various asymmetric transformations.

1.4 Deracemization (asymmetric transformation)

Deracemization is defined as the conversion of a racemate into a pure enantiomer or into a mixture in which one enantiomer is present in excess (or the conversion of a diastereoisomeric mixture into a single diastereoisomer or into a mixture in which one diastereoisomer is dominant.)[41] On the premise that enantiomers of the chiral substrate are freely interconvertible, i.e., can undergo racemization, deracemization can be achieved. To be suitable for deracemization, the system must (i) form a conglomerate and (ii) be racemizable in solution but retain its chirality in the solid phase. Although the mechanism behind deracemization is not yet fully elucidated, it is clear that many kinds of phenomena act cooperatively during this process, as shown in Figure 1.4. Depending on the technique, some phenomena can be ignored; for example, Ostwald ripening does not involve agglomeration and breakage.[42]

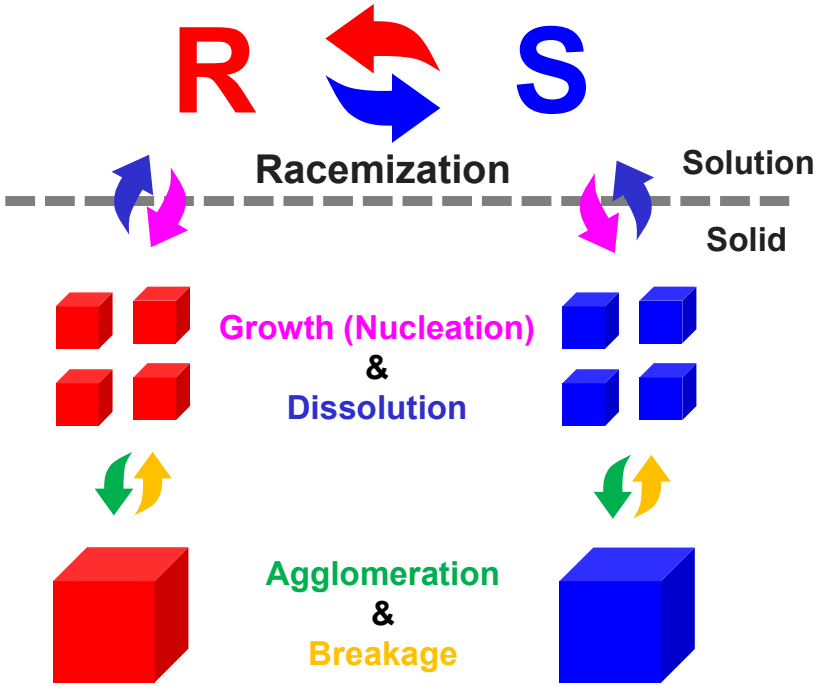

Figure 1.4 Schematic representation of the mechanism behind deracemization

Viedma ripening (VR):

Following the first experimental demonstration of symmetrical breaking of sodium chlorate ($NaClO_3$) by Kondepudi in 1990,[43] Viedma observed that the solid phase of a suspension of racemic $NaClO_3$, which was achiral in the solution phase but exhibited supramolecular chirality in the crystalline state, was brought to 100% ee by grinding with glass beads, through a process now known as Viedma ripening (VR) (Figure 1.5).[44]

Figure 1.5 Schematic representation of Viedma ripening. The grinding of conglomerate crystals with glass beads coupled with racemization in solution results in solid-phase deracemization.

In 2008, inspired by Viedma, Vlieg and coworkers demonstrated the principle of this process using a solid-phase chiral amino acid derivative in contact with a solution in which racemization occurs through the action of a base, and the amino acid was smoothly converted to a single chiral solid phase upon grinding with an abrasive material.[45] Triggered by this discovery, the deracemization of organic compounds by crystallization has been widely studied to date.

Ostwald ripening:

According to the IUPAC, Ostwald ripening is defined as the dissolution of small crystals or sol particles and the redeposition of the dissolved species on the surfaces of larger crystals or sol particles.[46] As a result of the Gibbs-Thomson effect, the smaller crystals in equilibrium with their saturated solution will dissolve to feed the growth of larger crystals. By itself, Ostwald ripening does not permit deracemization. However, it can lead to deracemization when it is applied to conglomerate crystals in a solution where they can racemize by free interconversion between enantiomers. Since the most thermodynamically stable state is a single crystal, enantiopure crystals, i.e., those with 100% *ee*, are generated. Indeed, the Ostwald ripening of chiral systems was demonstrated in a minireview by Vlieg and coworkers in 2009 (Figure 1.6).[39]

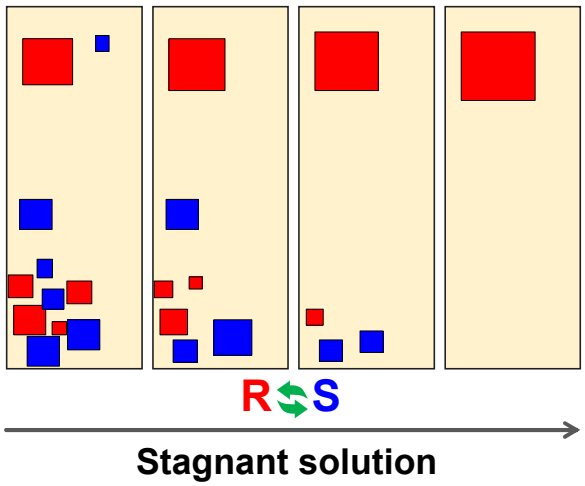

Figure 1.6 Ostwald ripening.

Temperature cycle-induced deracemization (TCID):

Temperature cycle-induced deracemization (TCID) can be considered as a VR-like deracemization using temperature fluctuations, usually without vigorous grinding by glass beads. From a historical viewpoint, it is a relatively new technique. In 2011, Viedma and Cintas reported that boiling suspensions of $NaClO_3$ could lead to deracemization, implying that dissolution/crystallization due to the temperature difference between the bottom and the rim of the flask plays an important role in deracemization.[47] Following this work, in 2013, Flood and Coquerel demonstrated the first example of TCID using a precursor of the drug compound paclobutrazol.[48] Compared to VR, TCID allows a shorter processing time because the temperature fluctuations allow the dissolution/crystallization cycle to be achieved on a larger scale.

Second-order asymmetric transformation (SOAT):

When a chiral substrate is racemizable in solution, stereoselective crystallization, such as diastereomeric adduct formation, allows the equilibration of enantiomers/diastereomers in solution and concurrent crystallization. As a result, all (or most) of a chiral substrate can be isolated as crystals. Such a 'crystallization-induced deracemization' is called a second-order asymmetric transformation (SOAT). This term may confuse many people since 'order' means just 'kind.' Indeed, the IUPAC Gold Book has used the phrase 'asymmetric transformation of the second kind' to refer to this process.[18] Based on the definition of a SOAT, this can include VR, Ostwald ripening, and TCID, and since all of these processes involve stereoselective crystallizations and the equilibration of enantiomers. However, recently, SOAT has only been used to refer to hybrid combinations of racemization and a seeded crystallization process, such as preferential crystallization, and it will be used like this hereafter to avoid confusion.

At the beginning of a SOAT process, a supersaturated solution is seeded with enantiopure crystals to trigger its stereoselective crystallization and generate the enantiomer with the same chirality as that of the seeds via crystal growth (and/or secondary nucleation) from the seed materials (Figure 1.7).

Stereoselective crystallization proceeds while the solution remains racemic due to racemization reactions. Since the mixture is initially far from the equilibrium seen in the final state, the process is generally a fast and productive process.

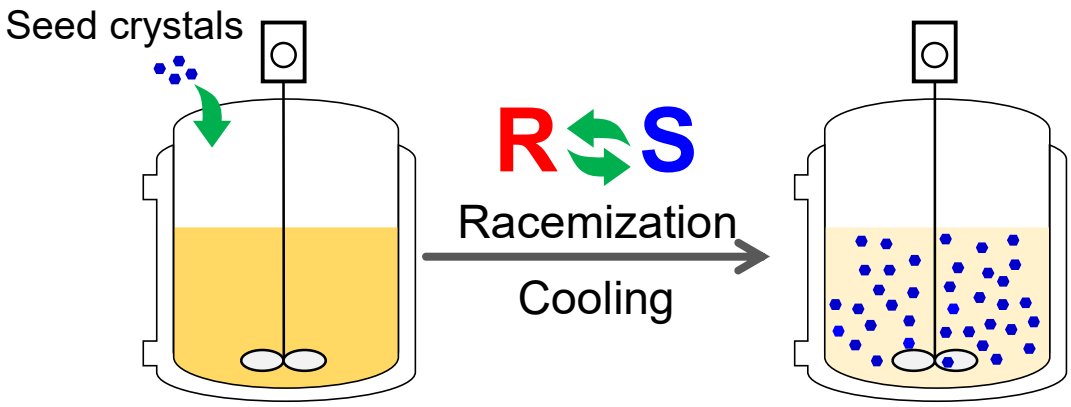

Figure 1.7 Schematic representation of a SOAT. The solution remains racemic during the crystallization.

2. Role of racemization kinetics on temperature cycle-induced deracemization

The content of this chapter has been published in a peer-reviewed journal:

Cryst. Growth Des. **2018**, *18*, 6417–6420. DOI: 10.1021/acs.cgd.8b01263

HAL ID: hal-01950306

2.1 Introduction

Conducting optimizations based on fundamental understanding of the resolution process is key to successful applications in industry. Among the different chiral-resolution techniques available to engineers,[35,49–51] deracemization is an attractive process because its theoretical yield is 100%, whereas the yields from other methods cannot exceed 50%. Although many techniques, for example, grinding,[52,53] ultrasound,[54] homogenization,[55] temperature cycling,[56,57] and microwaving,[58] have been applied in deracemization processes, TCID is considered to be the most promising technique from an industrial perspective because of its simplicity and applicability to a wide range of compounds. Hence, clarification of the key parameter(s) that control(s) deracemization processes through TCID is of great importance from an industrial viewpoint.

Many molecules have been deracemized, and several researchers have attempted to experimentally identify the key parameters that control these processes.[59–68] The results of these studies suggest that racemization and crystal-growth/dissolution rates are the essential factors that govern the efficiency of deracemization procedures. This observation is in good agreement with that of Iggland and Mazzotti, who focused on computational simulations of isothermal VR processes and showed that the ratio between these rates is the key criterion that controls the deracemization rate.[64] However, in the case of TCID, the dissolution/growth rates are mainly controlled by the temperature profiles. Consequently, when dissolution and crystal growth are smoothly performed, in principle, racemization rates should be the key parameter controlling the deracemization kinetics. In addition, it would be of great practical convenience if the racemization rate alone could be used as a good proxy for estimating deracemization.

Despite this precedent, the quantitative role of the racemization rate in deracemization kinetics has not yet been considered experimentally because of the difficulties associated with experimental systems. Indeed, most published deracemization studies focused on chiral compounds containing stereogenic centers that follow complicated deracemization kinetics involving the addition of another component (e.g., a base) into the system, thereby adding an additional level of complexity to the

problem.[69] The deracemization of atropisomers elegantly circumvents this issue.[53] Indeed, atropisomerism arises from axial chirality and is due to restricted rotation about a single bond. Accordingly, its racemization is a unimolecular process that should follow first-order reaction kinetics and can thus be characterized by a single parameter.

In this context, we prepared naphthamide **1** as a compound that racemizes via a simple process and forms in a conglomerate system. Indeed, compound **1** exhibits solid-state atropisomerism, whereas it spontaneously racemizes in solution. Naphthamide **1** has previously been reported by Sakamoto et al.,[70] and our sample was synthesized using a similar route (Scheme 2-1).

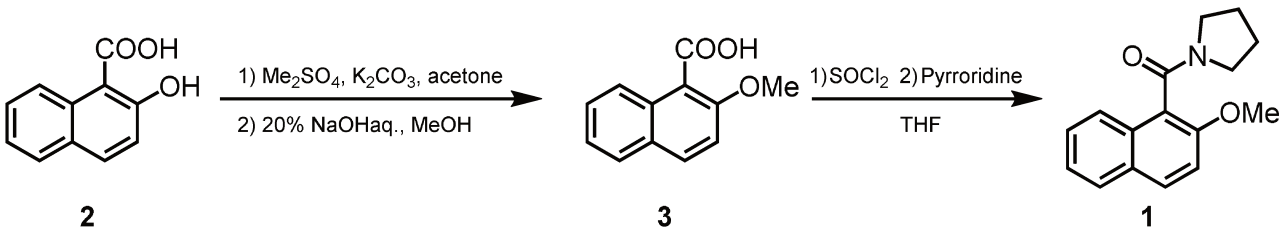

2 **3** **1**

Scheme 2-1 Synthesis of naphthamide 1.

2.2 Racemization kinetic constant and solubility

Sakamoto et al. reported the racemization rate constants (k_1 values) for **1** in methanol (MeOH), THF, and a 1:1 mixture of MeOH and THF.[70] Here, k_1 was measured in various solvents, including alcohols, ketones, nitriles, and ethers. A large single crystal (consisting of only one enantiomer) was dissolved in a solvent, and the time dependence of the optical rotation at 365 nm was recorded over a few hours using a polarimeter. As described by Ebbers et al.,[71] the racemization rate constant k_1 can be calculated from the loss of optical activity using Eq. (1):

$$(R) \underset{k_{-1}}{\overset{k_1}{\rightleftharpoons}} (S)$$

$$-\frac{d[R]}{dt} = k_1[R] - k_{-1}[S] \qquad \text{Eq. (1),}$$

where [*R*] and [*S*] are the concentrations of the respective enantiomers. Since this is a racemization reaction, the rate constants in the two directions are identical (i.e., $k_1 = k_{-1}$), and [*S*] can be replaced by $[R]_0-[R]$, where $[R]_0$ is the initial concentration of the *R* isomer, as in Eqs. (2)–(4):

$$-\frac{d[R]}{dt} = k_1(2[R]-[R]_0) \qquad \text{Eq. (2)},$$

$$-\int_0^t \frac{d[R]}{(2[R]-[R]_0)} = \int_0^t k_1\, dt \qquad \text{Eq. (3)},$$

$$-\ln\left[\frac{2[R]_t-[R]_0}{[R]_0}\right] = 2k_1 t \qquad \text{Eq. (4)}.$$

When $[R]_0$ is described by its optical rotation (α_0), then $2[R]_t-[R]_0$ can be replaced by the optical rotation at time *t* (α_t), as shown in Eq. (5):

$$-\ln\left[\frac{\alpha_t}{\alpha_0}\right] = k't \qquad \text{Eq. (5)}.$$

It should be noted that *k*' is twice the racemization rate constant (k_1). Consequently, the slope of $\ln[\alpha_t/\alpha_0]$ as a function of time can be used to determine the first-order racemization rate constant (k_1). The racemization rate was evaluated in terms of racemization rate constant (k_1). The solubilities and racemization rate constants (k_1) of **1** in the tested solvents are summarized in Table 2.1.

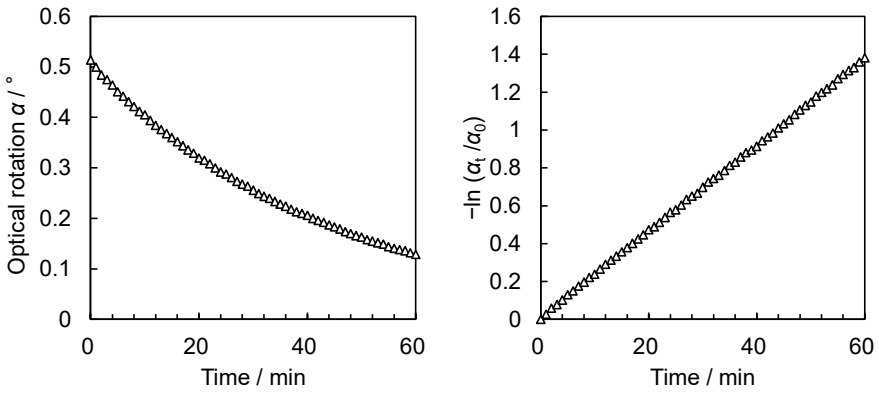

Figure 2.1 Example of the time-course plots of the optical rotation of 1 in acetonitrile at 20 °C (left) and a plot of the natural logarithm of the optical rotation at 365 nm as a function of time (right).

Generally, k_1 was higher in less-polar solvents. For example, k_1 increased linearly with increasing chain lengths of the nitrile solvents. Although the racemization rate constants were highest in ethereal

solvents, the solubility was relatively low. The racemization rate constants were much lower in alcohol solvents than in other types of solvent. These observations can be attributed to hydrogen bonding between the carbonyl oxygen of **1** and the solvent, which reduces the rate of racemization. Although Sakamoto et al. reported that **1** retains its chirality in MeOH through hydrogen-bonding interactions,[70] our systematic study revealed that the racemization rate of **1** depends on the solvent polarity, and this trend is particularly conspicuous within the same solvent series.

Table 2.1 Racemization rate constants (k_1) and solubilities of 1 in various solvents at 20 °C and at [1] 4 °C. [2] Reported by Sakamoto et al.. (a) isobutyronitrile (b) methyl tert-butyl ether (c) methyl isobutyl ketone

Solvent	Solubility / wt%	Racemization rate constant k_1 / min^{-1}	Half-life / min
MeOH	>25	2.64×10^{-3} (0.29×10^{-3}[1])	263 (2394[1])
2-Propanol	15.8	6.55×10^{-3}	106
*t*BuOH	10.5	8.55×10^{-3}	81
MeCN	27.0	11.1×10^{-3}	61
Propionitrile	29.0	20.2×10^{-3}	34
Butyronitrile	25.8	26.8×10^{-3}	26
*i*PrCN[a]	19.8	30.6×10^{-3}	23
Valeronitrile	22.1	38.9×10^{-3}	18
Diisopropyl ether	1.12	102×10^{-3}	7
MTBE[b]	1.35	80.5×10^{-3}	9
Dioxane	17.8	18.5×10^{-3} (15 °C)	38 (15 °C)
THF	-	21.4×10^{-3} (15 °C)[2]	16[2]
Acetone	20.0	28.3×10^{-3}	24
2-Butanone	19.5	47.0×10^{-3}	15
3-Pentanone	16.0	47.3×10^{-3}	15
MIBK[c]	11.5	49.1×10^{-3}	14

2.3 Crystal growth rate

To optimize the cooling rate of the TCID experiment, the crystal-growth rates of **1** in different solvents were evaluated by gravimetry. A supersaturated solution ($\beta = 1.09$), for which the supersaturation was determined by refractometry, was added to a precisely weighed amount of crystals (50.0 mg). The supersaturation was adjusted to the average of the solubilities at 20 and 25 °C. After a fixed period of crystal growth with gentle stirring, the crystals were filtered, washed, and carefully dried under vacuum for at least 5 h. The increase in mass was then determined using a weighing balance. The rate of increase of the crystal mass was plotted against the crystal-growth time, and the resulting slope was used to determine the gravimetric crystal-growth rate.

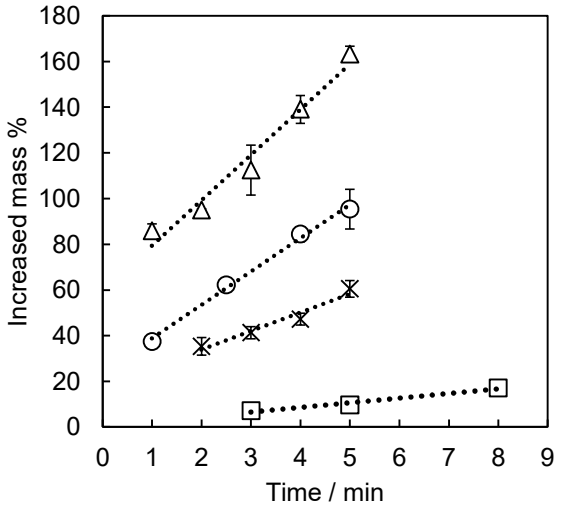

Figure 2.2 Relationship between the increase in mass of crystalline 1 and the time in: Δ, iPrCN; ○, tBuOH; ×, MIBK; and □, MTBE. Error bars represent standard errors.

2.4 Temperature cycle-induced deracemization

TCID experiments involving **1** were carried out in *t*BuOH, MTBE, MIBK, and *i*PrCN as described in Experimental details chapter. Compound **1** was efficiently deracemized through temperature cycling within a few days with final enantiomeric excesses (*ee*) greater than 90% in *t*BuOH, MTBE, MIBK, and *i*PrCN, regardless of any initial chiral bias (Figure 2.3). The crystal form obtained by deracemization was the same as that reported previously.[70]

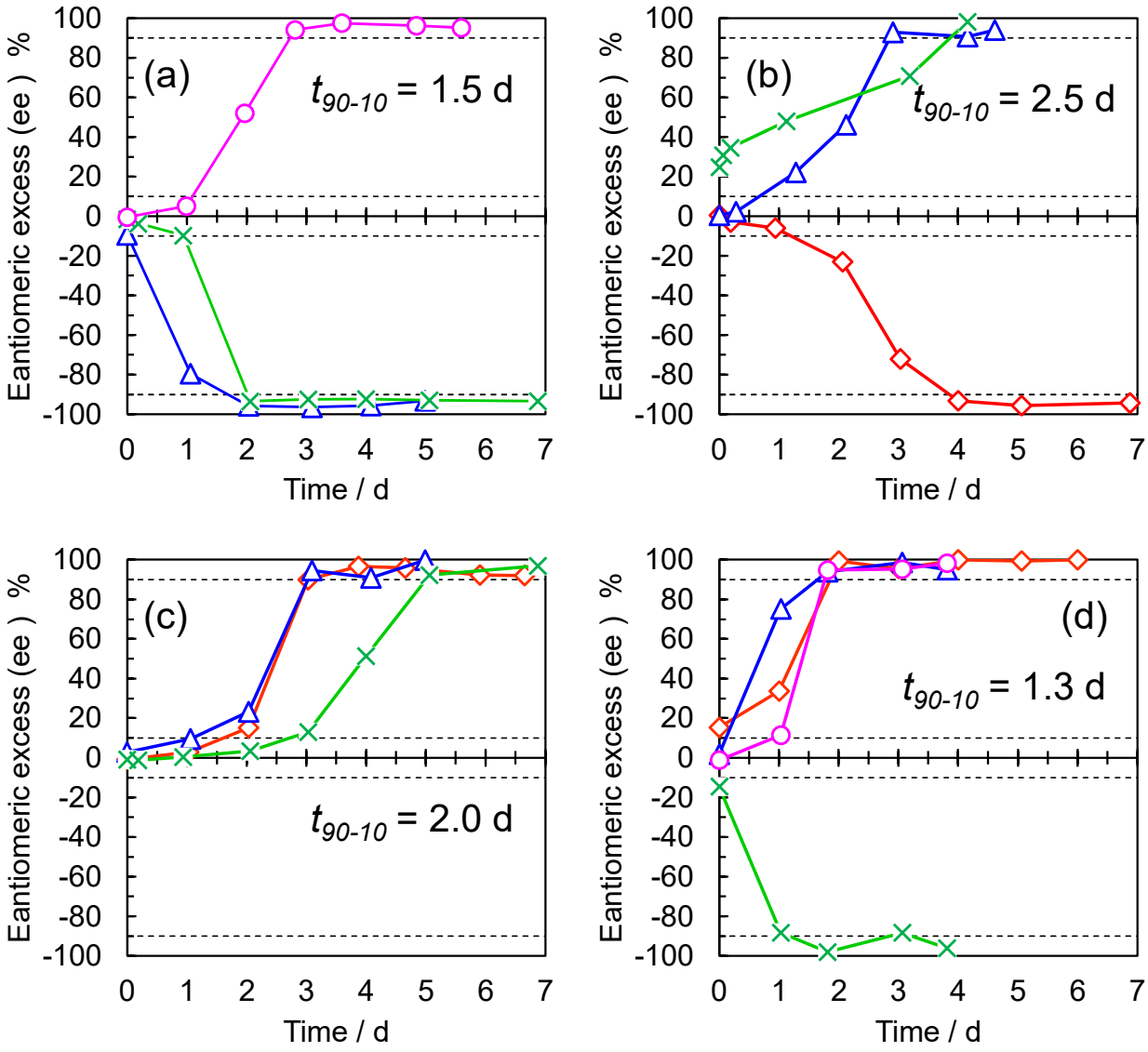

Figure 2.3 Enantiomeric excess (*ee*) values of the collected crystals of 1 as functions of time during the deracemization experiments, and the corresponding t_{90-10} values in (a) MIBK, (b) tBuOH, (c) iPrCN, and (d) MTBE. Each point includes uncertainty (< ± 1.5%) due to the polarimetry technique.

The change in enantiomeric excess as a function of time was sigmoidal in nature. This behavior is often observed in solid-state deracemizations. Except in the *i*PrCN system, the dominant enantiomer was determined by the initial chiral bias. Indeed, in the latter case, when the process was slightly (−)-enriched, deracemization occurred with the formation of the (opposite) (+)-isomer. Although we observed this phenomenon on two occasions, we are currently unable to provide an explanation for this observation.

2.5 Role of the racemization rate on the deracemization rate and productivity

To compare the deracemization rates under different conditions, in their computational work, Iggland and Mazzotti used the time required for the racemate (0% *ee*) to reach 90% *ee* to evaluate isothermal VR.[64] Here, we define the time required to reach 90% *ee* from a slightly enriched state (10% *ee*) to be $t_{90\text{-}10}$, which excludes unreproducible behavior often observed at the start of the deracemization process. For example, the chirality in the solid state can shift toward one enantiomer and then shift in the opposite direction. The $t_{90\text{-}10}$ values reported in Figure 2.3 are the averages of experiments conducted in triplicate. According to Iggland and Mazzotti, the deracemization kinetics are theoretically correlated with the ratio between the racemization rate and the crystal growth/dissolution rate.[64] However, as mentioned earlier, the cooling/heating steps were sufficiently slow to ensure that the suspension remained close to equilibrium; consequently, these steps are not rate limiting and can be excluded when considering the overall deracemization rate in the experiment. Thus, herein, we considered the influence of the racemization rate on the global deracemization rate.

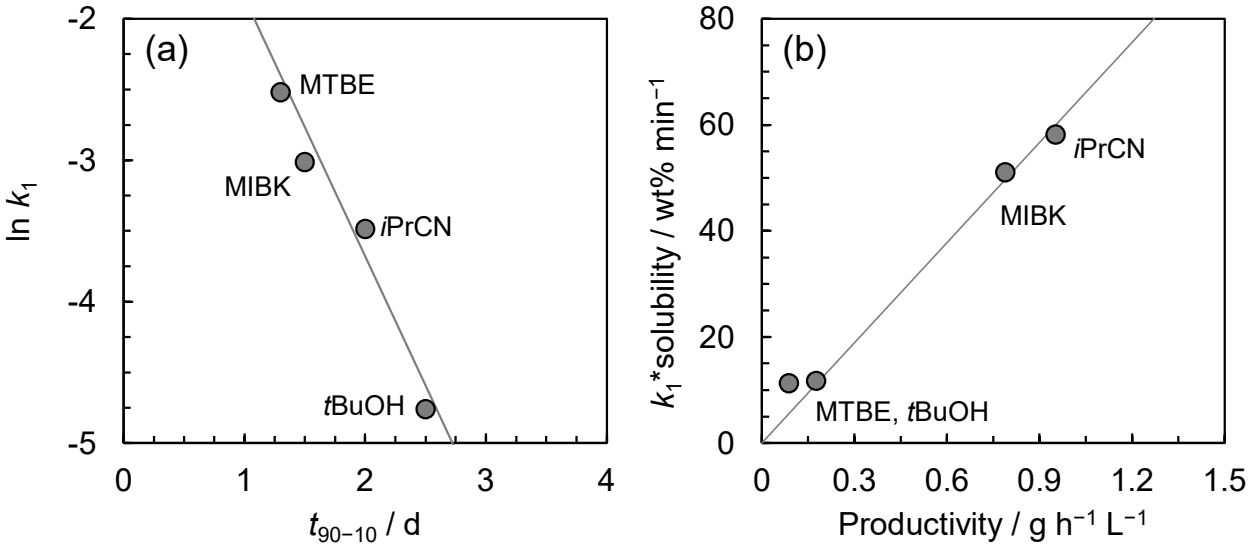

Figure 2.4 (a) Time required to achieve an *ee* of 90% (t_{90-10}) as a function of the natural logarithm of the racemization rate (k_1). (b) The product of k_1 and solubility as a function of the deracemization productivity.

Figure 2.4 displays a plot of the natural logarithm of k_1 as a function of $t_{90\text{-}10}$ using the experimental data collected for **1** in the four different solvents. The plot reveals that in the case of temperature cycling, the deracemization rate can be estimated by simply measuring the racemization rate. Contextualizing these results to real phenomena, these parameters can be intuitively interpreted as follows. Compounds that racemize slowly in solution will retain their enantioenrichment for long periods of time, and crystallization occurs with the same chirality before dissolution; therefore, deracemization will be sluggish. In contrast, this solution remained racemic during fast racemization, even during crystallization, which contributes to deracemization. This behavior qualitatively explains other results obtained experimentally for deracemization. For example, Breveglieri et al. recently reported the deracemization of *N*-(2-methylbenzylidene)phenylglycine amide (NMPA) with DBU through temperature cycling and concluded that a high operating temperature leads to fast deracemization.[57] The racemization of NMPA with DBU can be considered as a catalytic reaction, and consequently, the racemization rate is higher at higher operating temperatures. The faster deracemization kinetics at higher temperature for NMPA in DBU are, according to our interpretation, essentially due to the high racemization rate of NMPA. Moreover, we found that the deracemization productivity, which is defined by how much of the desired enantiomer is produced per unit time and volume of suspension, linearly correlates with the product of k_1 and solubility, as shown in Figure 2.4. In terms of the global outcome of the process, k_1 controls the deracemization time, and the solubility determines the scale of the symmetry breaking; hence, their product provides the productivity. For example, MTBE yields the fastest deracemization, but it is the worst medium in terms of productivity because of the poor solubility. This contrast illustrates that the order of the productivities differs from that of the deracemization rates. Thus, make this process operationally practical, it is very important to consider the balance between k_1 and solubility.

2.6 Conclusion

In summary, we report the first deracemization study of a single-component atropisomer through temperature cycling without the use of any racemization reagent. We also measured the racemization rates of the compound in different solvents to understand the influence of solvent on the overall deracemization rate. The results of our study suggest that the racemization rate (k_1) is the key parameter that determines the deracemization kinetics during temperature cycling. Nevertheless, when the productivity of the global process is important, the product of the racemization rate and solubility becomes the most relevant parameter. In this context, the process can be further clarified by studying the influence of impurities and the cooling rate on the process kinetics, in addition to the starting particle-size distribution.

3. Second-order asymmetric transformation of naphthamide

The content of this chapter has been published in a peer-reviewed journal:

Org. Process Res. Dev. **2019**, 23, 1197–1203. DOI: acs.oprd.9b00133

HAL ID: hal-02138812

3.1 Introduction

Preferential crystallization (PC) is a chiral resolution technique that can be applied to conglomerate-forming systems.[35] Notably, no racemization occurs during PC (i.e., enantiomers cannot interconvert), leading to the gradual enantioenrichment of the solution with the opposite enantiomer, which limits the yield of every operation. The theoretical maximum yield after recycling the mother liquor several times is 50%. By contrast, deracemization by crystallization is a more promising chiral separation technique, because although it also requires a conglomerate-forming system, it is performed under racemization conditions that steadily produce the desired enantiomer, leading to a theoretical yield of 100%.[72] In addition to this major advantage, deracemization by crystallization is quite easy. For example, temperature cycle-induced deracemization (TCID) converts a racemate of a substrate into a nearly enantiomerically pure solid phase without an external chiral source through temperature cycling.[11–13,56,57,73,74]

In Chapter 2, we discussed the TCID of napthamide **1** and its racemization rate (k_1), and we showed that the process productivity is proportional to the product of the racemization rate (k_1) and the solubility.

The productivity of a separation process is defined as the amount of enantiomer produced per unit time and unit volume of the crystallizer or suspension.[57,75]

$$Productivity = \frac{m_{crop} \times ee_{final} - m_{seeds}}{time \cdot volume} \quad \text{(Eq. 1)}$$

Here, m_{crop} and ee_{final} are the mass and the enantiomeric excess of the collected crystals, respectively, and m_{seeds} is the mass of the seed crystals. Although a few examples have exhibited good productivity (for example, the PC of baclofen[76] achieved an average productivity of 69 $gh^{-1}L^{-1}$ when considering the equilibration time before crystallization), the typical productivities of PC range from 10 to 20 $gh^{-1}L^{-1}$.[77,78] In comparison, the productivities of TCID processes are as low as 0.1–5.0 g h^{-1} L^{-1}.[57,79] Thus, although TCID can double the theoretical yield, the productivity of the process is almost an order of magnitude lower than that of PC.

The low productivity of TCID is obviously due to the associated long process times. Indeed, the usual minimum process duration for TCID is approximately 10 h.[13,54,57,80] In contrast, PC runs typically involve rapid cooling; thus, the process times are much shorter. Correspondingly, shortening process times is important for significantly improving the process productivities and achieving a process with high productivity.

The scaling up of PC often leads to problems in sub-operations, even when chiral crystallization is effective. In particular, the filtration step can affect the feasibility, and occasionally this kind of problem causes PC to fail. For example, laboratory-scale filtrations can usually be completed in a reasonable amount of time, but large-scale filtrations require much longer. The PC process normally incorporates a quick filtration after the end of the entrainment because a longer crystallization period could trigger nucleation of the opposite enantiomer and reduce the optical purity of the crop. Therefore, the time required for the filtration of a large-scale system could constitute a critical problem. In contrast, deracemization processes generally do not face this problem due to the steady interconversion of the enantiomers in solution. Moreover, the supersaturation of both enantiomers is maintained close to 1; thus, the probability of the nucleation of the opposite enantiomer decreases. This feature eliminates this obstacle in the scaling up of the process and makes this process more applicable in industry.

As described in Chapter 1, second-order asymmetric transformation (SOAT) is defined as a crystallization-induced asymmetric transformation during which a racemate is converted into either a pure enantiomer or a mixture in which one enantiomer is present in excess.[41]

As a hybrid of stereoselective crystallization and deracemization, SOAT offers great promise for achieving both a high yield and high productivity. To the best of our knowledge, there have been relatively few reports on SOAT processes, and no studies have investigated the productivity of such processes.[81–108] In this chapter, we examined the application of the SOAT process to naphthamide **1,** a conglomerate-forming system that exhibits solid-state atropisomerism (i.e., it spontaneously racemizes in solution) at two different scales. In addition, we show that the SOAT of this compound

is more productive than is regular TCID, even if the two processes are comparable in terms of the relationships between their homogeneous and heterogeneous equilibria.[109]

3.2 Solubility and racemization kinetics

In terms of practicality of the following experiments, the solubility of **1** in a solvent should be moderate (10-20 wt%). The solubility of **1** in a 45/55 (wt/wt) mixture of cyclohexane and ethyl acetate (Certified AR for Analysis, Fisher Chemical, France), an azeotropic mixture, was measured by a gravimetric method from 10–60 °C. The temperature was controlled by a thermostat (F25-HL Cryostat, JULABO GmbH, Germany). The racemization kinetic constants (k_1) of **1** from 10–45 °C were also measured over time at 365 nm using a polarimeter (P-2000, Jasco France, France) with a Hg lamp. Figure 3.1 shows the solubilities and k_1 values of **1** as functions of temperature in an azeotropic mixture of ethyl acetate and cyclohexane (45/55 wt/wt).

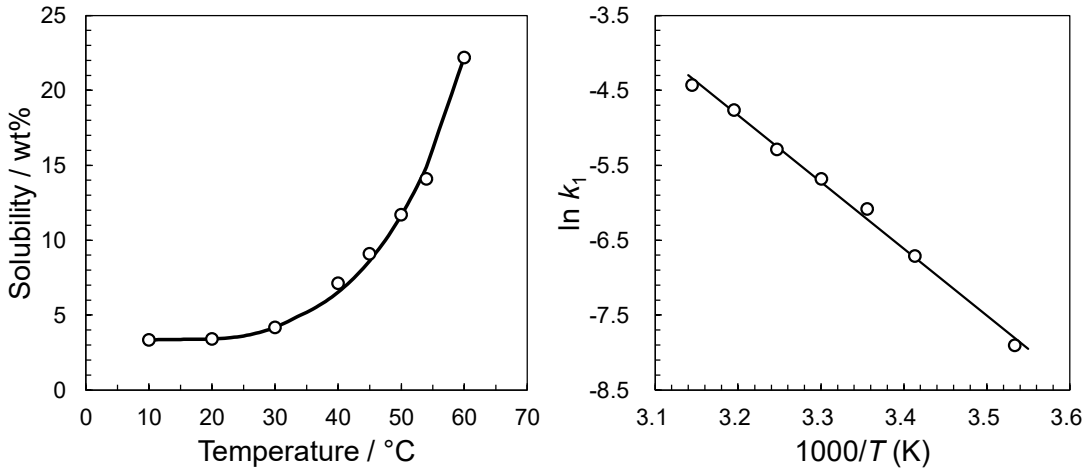

Figure 3.1 (Left) Solubility curve and (Right) Arrhenius plot of racemization rate constants of 1 in an azeotropic mixture of cyclohexane and ethyl acetate (45/55, wt/wt).

The variation in solubility from 10–30 °C is small, but solubility increases dramatically above 30 °C. This behavior suggests the existence of a metastable miscibility gap at higher or lower temperatures, which is also called submerged liquid demixing or the metastable oiling-out phenomenon.[110]

Therefore, seeded crystallization is suitable for this compound to avoid liquid demixing, which may cause high supersaturation in one of the two liquids and thus uncontrolled crystallization. The racemization kinetic constants (k_1 values) obtained by polarimetry measurements have been used to plot an Arrhenius graph (Figure 3.1), and the Gibbs free energy of activation ($\Delta G^{\ddagger}$) was found to be 17.1 kcal·mol^{-1}. In general, a torsional rotation energy barrier lower than 20–25 kcal·mol^{-1} will result in interconversion within a few hours near room temperature.[111] Thus, this value indicates that racemization in the solution is sufficiently fast to facilitate the development of a deracemization process over a reasonable period of time. The details of the solubility data and k_1 are given in Table 3.1

Table 3.1 Mass fraction solubility (*c*), mole fraction solubility (*x*), racemization kinetic constants (k_1), and half-life time ($t_{1/2}$) of 1 in an azeotropic mixture of cyclohexane and ethyl acetate. [a] standard uncertainty on *x*.

T / °C	c / wt% (s.d.)	x	$u_r(x)$%[a]	k_1 / 10^{-3} s^{-1}	$t_{1/2}$ / s
10	3.34 (0.16)	0.0118	4.7	0.37	1874
20	3.41 (0.13)	0.0120	3.7	1.22	569
25	-	-	-	2.28	304
30	4.19 (0.17)	0.0149	4.1	3.42	203
35	-	-	-	5.06	137
40	7.14 (0.03)	0.0258	0.4	8.54	81
45	9.10 (0.07)	0.0334	0.8	11.9	58
50	11.70 (0.09)	0.0437	0.8	-	-
54	14.10 (0.07)	0.0535	0.5	-	-
60	22.20 (0.05)	0.0898	0.2	-	-

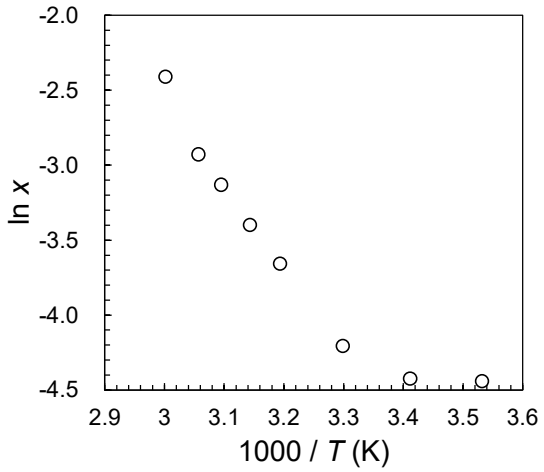

Figure 3.2 Experimental plot of ln *x* of 1 vs. 1/*T* in an azeotropic mixture of ethyl acetate and cyclohexane.

3.3 Deracemization experiments: TCID and SOAT

The TCID of **1** was performed using the following procedure. Compound **1** was completely dissolved by heating in 10 mL of an azeotropic mixture of ethyl acetate and cyclohexane (55/45, wt/wt) in a 30-mL screw vial that contained a cross-shaped Teflon-coated stir bar. Subsequently, the solution was cooled to 10–20 °C to induce spontaneous crystallization. Then, the suspension was maintained at 20 °C for 30 min to allow it to reach equilibrium. The heterogeneous mixture was stirred under the temperature cycling conditions shown in Figure 3.3 for a maximum of 10 d. To confirm the scalability of the process, we performed the TCID of **1** at 4 different levels of suspension density (ρ), namely, 14.4, 36.0, 72.0, and 144 mg mL^{-1}. Since the temperature cycle between 20 and 30 °C gives a 7.2-mg mL^{-1} dissolution-crystallization cycle, 50, 20, 10, and 5% of the crystals were deliberately dissolved during the heating step. For the off-line monitoring of the deracemization experiments involving **1**, a small amount (~30 μL) of the suspension was drawn off and filtered through an 8φ filter paper in a Kiriyama Rohto VB-8 funnel. The collected crystals were dried under vacuum, weighed, and then dissolved in MeOH (1.200 mL, HPLC grade) at 4 °C. The enantiomeric excess was determined by comparing the optical rotation at 365 nm and 4 °C with the previously determined specific optical rotation ($[\alpha]^4_{365}$= 662.3 (MeOH)).[79]

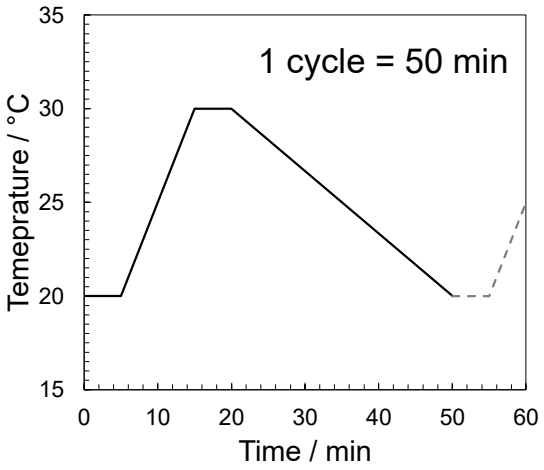

Figure 3.3 Temperature profile applied in the TCID experiments.

The SOAT process of **1** was carried out using the procedure described in Experimental chapter. The two types of cooling profiles during crystallization are shown in Figure 3.4, which are hereafter referred to as cooling profiles A and B. The experimental conditions are summarized in Table 3.2.

Table 3.2 Experimental conditions for the SOAT of 1 in a 45/55 (wt/wt) mixture of cyclohexane and ethyl acetate.

Run	Cooling profile	**1** /g	solvent / g	S / wt%	Seed / mg	$T_{initial}$ / °C	T_{final}/ °C	Duration / min
1	A	1.425	5.00	22.2	27.0	60	30	82
2	A	1.426	5.00	22.2	32.4	60	30	82
3	A	1.422	5.00	22.2	33.0	60	30	82
4	B	1.428	5.01	22.2	10.9	60	30	85
5	B	1.424	5.00	22.2	21.5	60	30	82
6	B	1.427	5.01	22.2	30.8	60	30	83
7	B	1.428	5.01	22.2	10.3	60	30	81
8	B	9.990	35.01	22.2	60.8	60	30	89
9	B	9.984	35.00	22.2	143.8	60	30	84
10	B	9.945	34.96	22.2	35.1	60	30	85
11	A	9.989	35.00	22.2	41.1	60	30	85

In cooling profile A, the temperature decreases linearly as a function of time (Figure 3.4), and the C_T/C_{30} ratio, with C_T and C_{30} being the gravimetric solubilities at T and 30 °C, respectively, changes drastically at the beginning of the process. Due to the solubility change, the supersaturation of the

solution is expected to increase dramatically, and primary nucleation of the opposite enantiomer can occur. In contrast, as seen in cooling profile B, the solubility linearly decreases with time in order to achieve a constant rate of crystal growth when the cooling rate is sufficiently slow to reach the solubility equilibrium at a specific temperature. In general, the rate of crystal growth in the fast cooling process depends on the diffusion and/or surface integration behavior of the molecule; therefore, this rate cannot be considered to be constant.

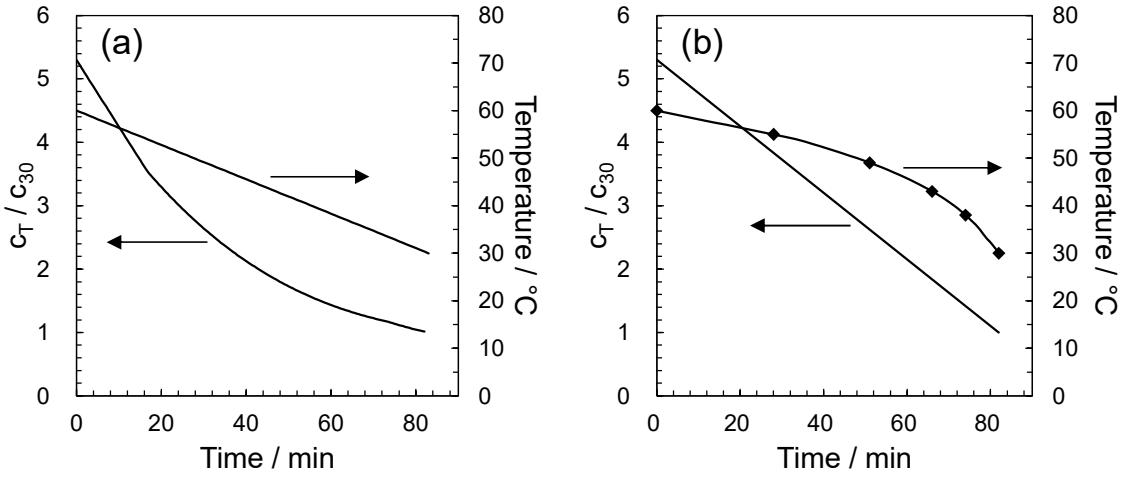

Figure 3.4 Two types of cooling profiles applied in the SOAT of 1. (A) Linear cooling. (B) Solubility-controlled cooling; c_T: saturated concentration at temperature T[°C]. Symbols (♦) in profile B are actual input points used in the temperature program of the thermostat.

3.4 Comparison of productivity: TCID vs SOAT

In the present study, the productivity was calculated using Eq. (1), in which the volume of the solution (calculated using a solvent density of 0.856 g mL^{-1} and the measured mass at 20 °C) was used instead of the suspension volume. To compare the efficiency of TCID to that of SOAT, the yields were calculated using Eq. (2):

$$\text{Yield}[\%]=\frac{m_{crop}\times ee_{final}-m_{seeds}}{m-m_{solute,\,final}}\times 100 \quad \text{(Eq. 2)}$$

where m and $m_{solute,\,final}$ represent the total mass of **1** and the mass of the solute in the saturated solution at the final temperature, respectively.

In general, the crystallization yield does not consider the mass of solute remaining in solution since it can vary depending on the operating conditions. The thorough optimization of the operating conditions that would therefore be necessary to compare such factors for different processes is beyond the scope of this study. The yield should be 100% when the mass of collected crystals is the same as the theoretically obtainable mass (i.e., taking into account the mass of the solute that remains solvated at the final temperature). Thus, the yield can be considered a factor in determining the process efficiency.

Figure 3.5 displays the enantiomeric excesses (*ee*s) of the crystals of **1** collected during the TCID experiments as a function of time, while Table 3.3 summarizes the suspension density, the deracemization time (which is the time required to reach 95%*ee* from 0%*ee*), and the process productivity. As shown in Figure 3.5, a higher suspension density resulted in a longer deracemization time. Although the process productivity for the solution with a suspension density of 144 mg·mL^{-1} was 10% lower those of the other cases, there was no significant difference in this range of suspension densities. Thus, the process productivity of a TCID can be regarded as an independent factor affecting suspension densities in the range of 10–150 mg·mL^{-1}. Suspension densities above this range may disturb the homogeneity of the system, and the suspension density would not be independent of the

process productivity. Hereafter, the average value, 0.67 $g \cdot h^{-1} \cdot L^{-1}$, is used as the process productivity of TCID for comparison.

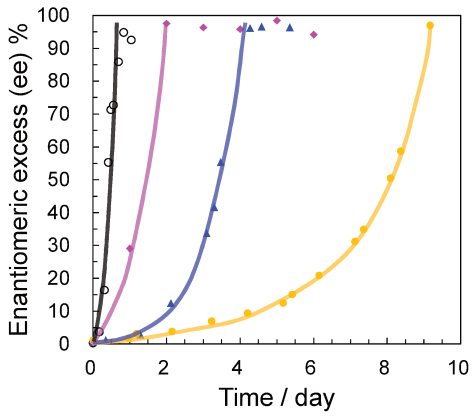

Figure 3.5 The enantiomeric excess of the collected crystals of 1 as a function of time during temperature cycle deracemization experiments in an azeotropic mixture of ethyl acetate and cyclohexane. Colors indicate the suspension density. Black: 14.4 $mg \cdot mL^{-1}$, magenta: 36.0 $mg \cdot mL^{-1}$, blue: 72.0 $mg \cdot mL^{-1}$, yellow: 144 $mg \cdot mL^{-1}$. The lines are a guide for the eye.

Table 3.3 Summary of the suspension density, deracemization time, and process productivity.

Suspension density ρ / $mg \cdot mL^{-1}$	Deracemization time / h	ee_{final}[%]	Productivity / $g \cdot h^{-1} \cdot L^{-1}$	Yield[%]
14.4	20	96	0.68	>95
36.0	48	98	0.71	>95
72.0	102	97	0.67	>95
144	220	97	0.62	>95

The experimental results of the SOAT of **1** are summarized in Table 3.4.

Table 3.4 Summary of the experimental results of the SOAT crystallization.

Run	Cooling profile	m_{crop} / g	ee_{final} [%]	Productivity / g h^{-1} L^{-1}	Yield [%]
1	A	1.208	4	3	2
2	A	1.211	26	35	23
3	A	1.220	5	3.5	<1
4	B	1.205	87	125	86
5	B	1.219	93	139	92
6	B	1.206	97	141	94
7	B	1.188	89	133	87
8	B	8.317	77	104	75
9	B	8.360	83	118	80
10	B	8.432	85	124	85
11	A	8.646	51	75	51

The mass of the crystals collected after Runs 1–3 (performed using linear cooling) was almost equal to the maximum value, i.e., the crystallized mass accounts for the solubility difference between the initial and final temperature. However, the average enantiomeric excess was only 12%. Because of this low enantiomeric excess, the yield was also low. Although the productivities of Runs 1–3 were higher than those obtained for TCID in the same solvent (0.67 g h^{-1} L^{-1}), additional enantio-purification would be needed to achieve enantiopurity, which is undesirable.

To understand the reason for this low enantiomeric excess, we performed a 10-g scale SOAT experiment (Run 11 in Table 3.2 and Table 3.4) and monitored the enantiomeric excess of the crystal during this process. As shown in Figure 3.6, the enantiomeric excess in the crystal initially decreases during the experiment. Because the C_T/C_{30} ratio decreases rather abruptly in this temperature region (Figure 3.4), uncontrolled primary nucleation of the opposite enantiomer likely occurs upon cooling. This is further supported by Figure 3.6, which depicts the supersaturation profile of the solution and shows that the supersaturation remained quite high (~1.2) during this process. The increase in the supersaturation at the end of the experiment is likely due to the crystallization rate decreasing at lower temperatures as it cannot adapt to the corresponding temperature change.

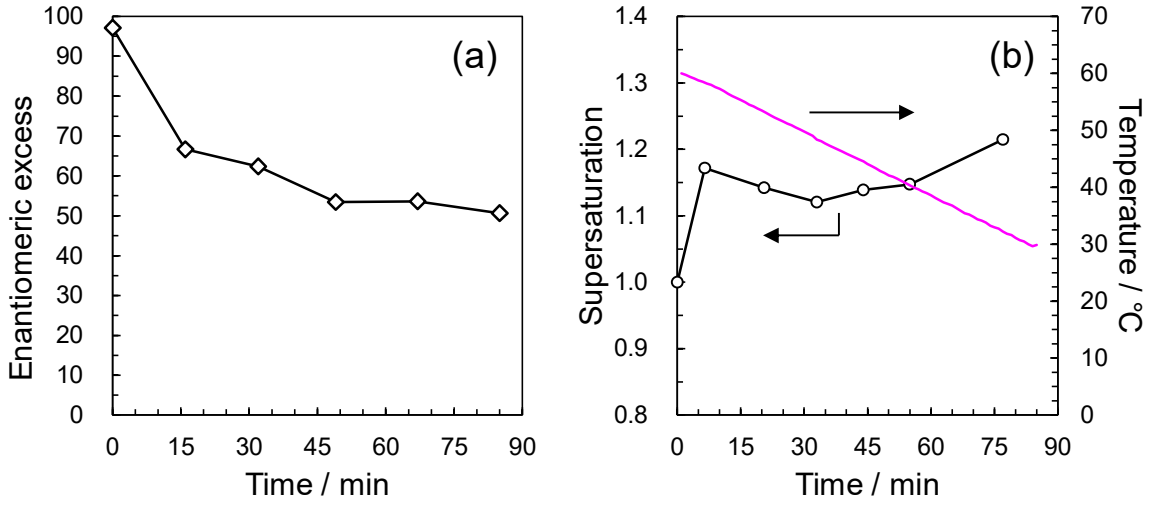

Figure 3.6 (a) Enantiomeric excess (*ee*) values of the collected crystals of compound 1. (b) Temperature profile of the SOAT experiments with linear cooling, and supersaturation as a function of time during the SOAT experiments with linear cooling (cooling profile A).

In contrast, the crystals obtained by solubility-controlled cooling (cooling profile B) exhibited high enantiomeric excesses (Runs 4–11, Table 3.4) and showed moderate yields (75–95%) compared to those obtained by TCID (> 99%). The absolute configuration of the resulting crystals was also identical to that of the seed crystals. Accordingly, the monitoring of the enantiomeric excess of the crystals (Figure 3.7) showed that the initial enantiomeric excess of the seeds was almost constant throughout the process. The cooling profile applied in these experiments implies a slow cooling rate at the beginning of the process, which reduces the primary nucleation of the opposite enantiomer (Figure 3.7). The cooling profile maintains a supersaturation close to 1.0 during the entire process (the crystal growth of the seeds is sufficiently fast to compensate for the moderate increase in supersaturation).

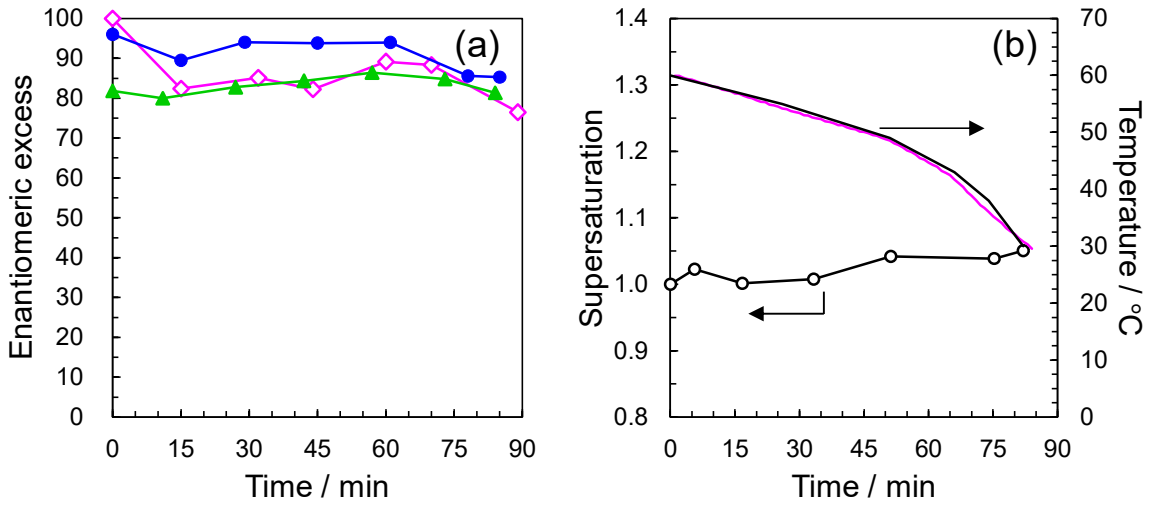

Figure 3.7 (a) Enantiomeric excess (*ee*) values of the collected crystals of 1. The lines correspond to Runs 8, 9, and 10. (b) Temperature profile of the SOAT experiments with solubility-controlled cooling (black line: ideal profile, magenta line: observed profile), and supersaturation as a function of time during the SOAT experiments with solubility-controlled cooling (cooling profile B).

The average productivity of the TCID for **1** was 0.67 g h^{-1} L^{-1}, while that of the SOAT on the same scale (i.e., Runs 4–7) was 135 g h^{-1} L^{-1}. This productivity difference is a result of the process time. Although the process time depends on the scale of the crystallizer, TCID is generally performed over

a period of several hours to a few days, whereas SOAT can be performed in a few hours because it requires only a single cooling process. Moreover, for the 10-g scale experiment (Run 8−10), without sophisticated optimization (i.e., the mass of the compound and solvent were increased proportionally), the time required for the process remained the same, and the decrease in productivity was only 10% compared to the 1-g scale process. Therefore, scaling-up for industrial applications is expected to be relatively easy.

Figure 3.8 shows an SEM image of a crop of crystals after cooling profile A. The crystals exhibited a size distribution of 10−100 μm, and small particles were adhered to the crystals. These small particles could have been produced by primary nucleation during the process, implying that primary nucleation frequently occurred during cooling profile A. Since the chirality of the primary nucleation could not be controlled, the particles formed by nucleation included both enantiomers. Therefore, the enantiomeric excess dropped during cooling profile A. In contrast, relatively large crystals (100−1000 μm) were found in the crop after cooling profile B, as shown in Figure 3.8. These crystals can be regarded as grown seeded crystals. As abrasions were visible on the large crystals, abrasion might also occur during this process. Since abrasion produces small crystals with the same chirality as the original crystals, the resulting crystals do not show a lower enantiomeric excess. Smaller crystals could be generated by the abrasion of large crystals or by secondary nucleation.

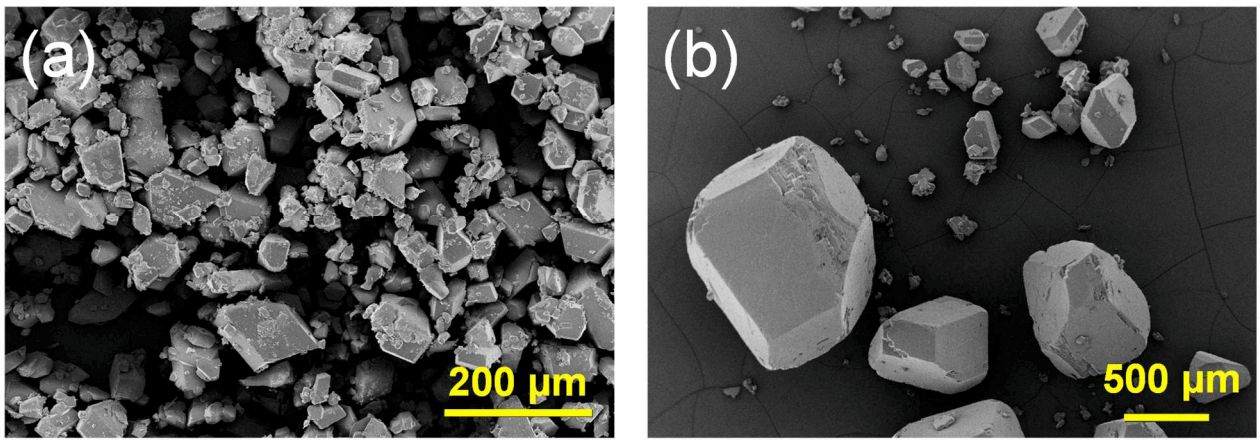

Figure 3.8 (a) SEM images of crystals collected after (a) cooling profile A and (b) cooling profile B.

3.5 Conclusion

We performed a SOAT on atropoisomeric naphthamide **1**, which exhibits spontaneous racemization in solution in the absence of a racemization reagent, with two different temperature profiles at 1-g and 10-g scales. The monitoring of the supersaturation of the solution and the enantiomeric excess of the solid phase upon cooling highlighted that so-called "solubility-controlled cooling" is better suited to producing crystals with high *ee*s. Moreover, we showed that the productivity of the SOAT is considerably higher than that of the TCID. The present study is the first to compare the productivities of SOAT and TCID for the same compound, naphthamide 1. In addition, we found that scaling up by a factor of 10 was feasible. Although SOAT requires enantiomerically pure seed crystals, it could be use as part of an efficient purification process in the future. For example, TCID could be used to prepare enantiopure crystals, which could then be used as seed crystals in a SOAT process. Alternatively, a continuous SOAT process could be envisaged as a more productive technique than TCID.

4. Second-order asymmetric transformation in a complex quaternary system using a phase diagram

The content of this chapter has been published in a peer-reviewed journal:

Chem. Eur. J. **2019**. *25*, 13890-13898. DOI: 10.1002/chem.201903338

Selected as the front cover and a Hot Paper

HAL ID: hal-02276778

4.1 Introduction

Phase diagrams are important tools for understanding and controlling crystallization. Indeed, the construction of a phase diagram is essential for rationally (i) determining the appropriate crystallization conditions for molecules exhibiting multiple solid phases, (ii) assessing the thermodynamic stability of their solid phases, (iii) and controlling supersaturation.[112–114] Recently, our group demonstrated that PC could be applied to a metastable conglomerate of diprophylline, which crystallizes in various crystalline forms depending on the conditions.[115] However, the utility of such an approach applying phase diagram investigations for deracemization has not yet been reported. While deracemization is a well-developed chiral resolution technique, its widespread use faces limitations. For example, it is suitable only for conglomerate-forming systems, i.e., 5-10% of racemic crystals.[22] Since racemization of the substrate is necessary for the deracemization process, the gap between the thermodynamic equilibria in the process must be tuned to design reaction conditions for efficient deracemization. For advanced industrial applications, the availability of model studies is crucial for facile process modeling. The present work aims to serve as a model study for the use of a phase diagram-based approach for the deracemization of molecules that exhibit a complex solid-phase landscape.

In the present study, we characterized two new solid phases of atropisomeric naphthamide **4**, shown in Figure 4.1, using SC-XRD, DSC, and XRPD measurements and constructed a quaternary phase diagram of **4** in a mixture of methanol (MeOH) and water (H_2O) using XRPD and solubility measurements.

Furthermore, we studied the impact of temperature on the racemic isoplethal section. Based on the conditions obtained from the phase diagram study, we successfully performed the chiral resolution of **1** by a SOAT in a MeOH/H_2O solution and achieved up to 97 % ee and a productivity of 6.5 g h^{-1} L^{-1}.

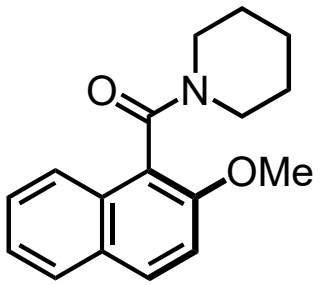

Figure 4.1 Chemical structure of atropisomeric naphthamide 4.

4.2 Three of crystal structures of naphthamide

Naphthamide **4** was synthesized using our method described in Experimental deteils, with a slight modification. The conversion of 2-hydroxy-1-naphthoic acid **2** (Sigma-Aldrich) to 2-methoxy-1-naphthoic acid **3** was carried out in 2 steps, and the condensation of the prepared 2-methoxy naphthoic acid with piperidine afforded **4**. The methods for the preparation of the conglomerate (C), the racemate (R), and the MeOH solvated racemic compound (Me) are summarized in Table 4.1.

Table 4.1 Preparation methods for the three solid phases of 4. [a] Ethanol, isopropyl alcohol, *tert*-butyl alcohol, acetonitrile, isobutyronitrile, methyl *tert*-butyl ether, tetrahydrofuran, acetone, and methyl *iso*-butyl ketone

Solid phase	Preparation method
C	Slow evaporation from conventional solvents[a]
Rac	Cooling crystallization from a $CHCl_3$/heptane (1/1, v/v) mixture or slow evaporation from a MeOH/H_2O (8/2, v/v) mixture
Me	Cooling crystallization or slow evaporation from a solution in MeOH

In 2005, Sakamoto et al. reported the crystal structure of the first form of **4**, designated C,[116] which can be prepared from solutions of **4** in many conventional solvents, except MeOH, by slow evaporation. The space group of C is $P2_12_12_1$, and the crystals form a conglomerate. The racemic compound, Rac, could be obtained in the first crop by cooling crystallization from a mixture of chloroform and heptane (1/1, v/v). Indeed, after collection of the Rac by filtration, only C crystallized from the filtrate. Rac can also be prepared by suspending any crystal form in a mixture of MeOH/H_2O (70/30, v/v) at 15 °C. As the melting point of Rac is 12 °C lower than that of the racemate of C, it could be considered less stable than C at high temperature in the binary system.

Furthermore, a comparison between the enthalpies of fusion (ΔH_{fus} values) also supports the order of stability. A <1-1> racemic MeOH solvate could also be prepared. The deposited crystals appeared highly transparent in the solution, and after filtration, the surface of the crystals desolvated and converted to C. The desolvation temperature of Me was determined by TGA-DSC-MS analysis (Figure 4.2). The incorporated MeOH molecules were released at 50.4 °C, and Me was converted to

C and/or Rac depending on the heating rate. XRPD measurements confirmed that a structurally pure sample of each phase could be prepared (Figure 4.3).

Table 4.2 Thermochemical properties of the four solid phases of 4. C: {(+) and (−)}, Rac, and Me.

	C	Rac	Me
Thermodynamic stability	Stable	Slowly transforms to C at high temperature	The surface can be desolvated under ambient conditions
Melting point / °C	111.2	99.4	50.4
ΔH_{fus} / kJ·mol^{-1}	24.8	20.8	desolvation

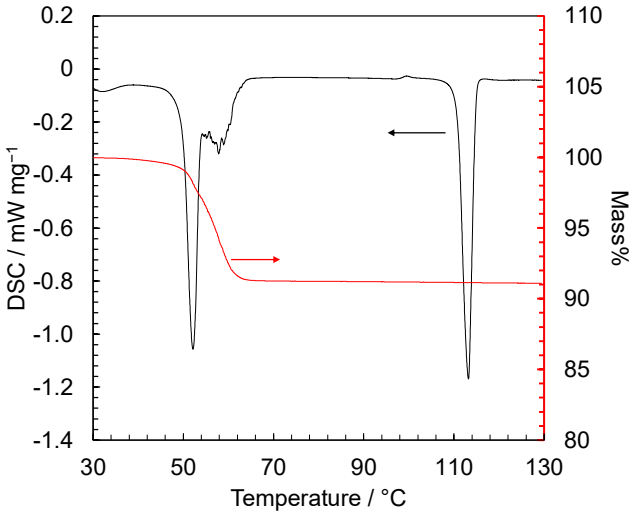

Figure 4.2 TGA/DSC curves of Me.

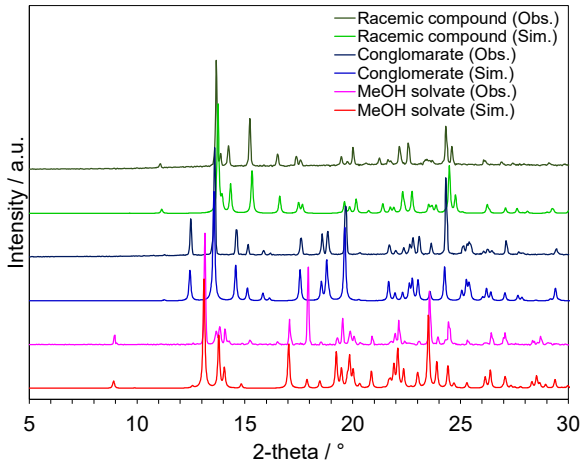

Figure 4.3 XRPD patterns of the three crystal forms of 4.

The crystallographic data for C, Rac, and Me of **4** are summarized in Table 4.3 for comparison. The data for C from Sakamoto's report, ref code NATQEF, have been included. Rac and Me correspond to racemic compounds. The ORTEP representations of Rac and Me are shown in Figure 4.4a and b, respectively. The overlaid molecular structures of Rac and Me (Figure 4.4c) indicate that the conformations in the two solid phases are almost identical. The major difference between Rac and C was in the piperidyl residues, as shown in Figure 4.4d. In both solid phases, the piperidyl groups exist in the chair conformation. However, the conformations of the piperidine rings are opposite, with the two piperidyl rings related through a chair flip.

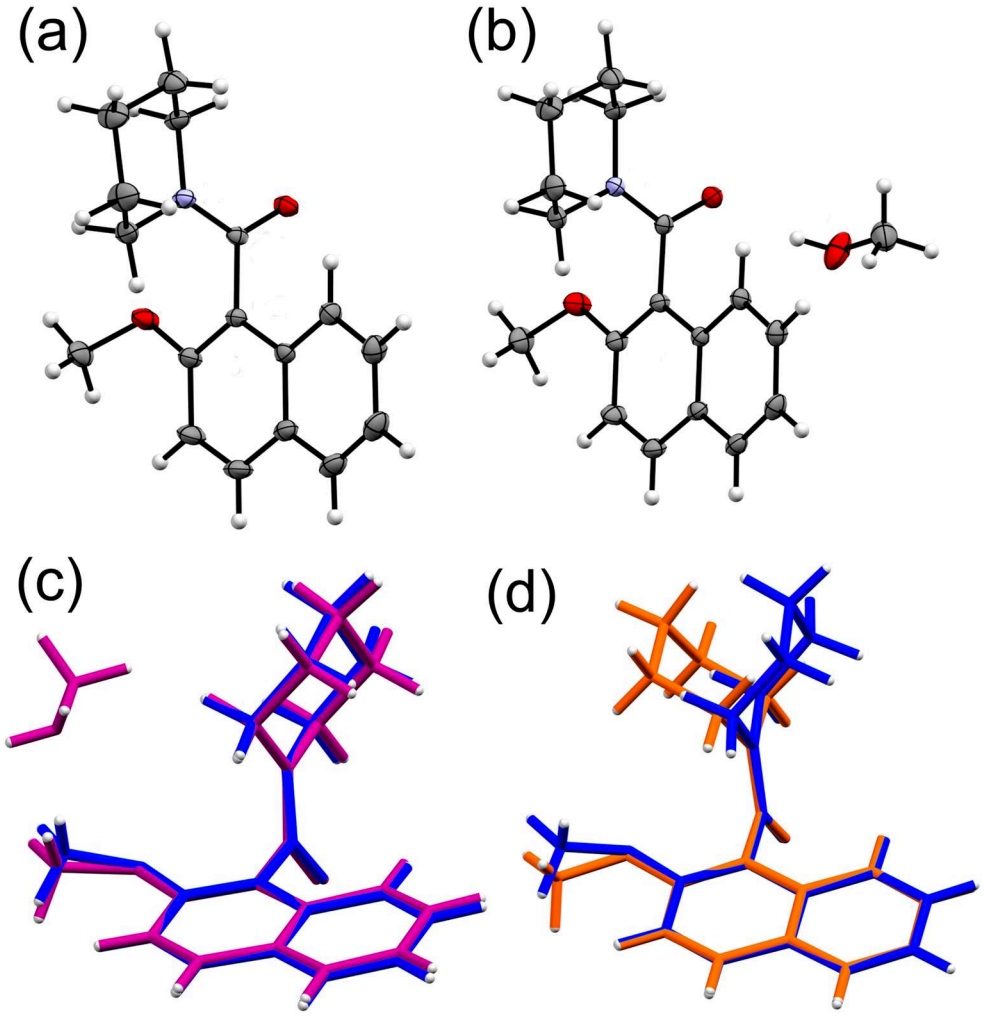

Figure 4.4 ORTEP representations of the (*R*)-enantiomer (a) in Rac and (b) in Me of 4 at 150 K. Thermal ellipsoids are displayed at 50% probability. Overlaid molecular structures of (c) Rac (blue) and Me (magenta) and of (d) Rac (blue) and C (orange).

Table 4.3 Crystallographic data of C, Rac, and Me. [a]Reported by Sakamoto et al. Ref code: NATQEF.

Name	C[a]	Rac	Me
Chemical formula	$C_{17}H_{19}NO_2$	$C_{17}H_{19}NO_2$	$C_{17}H_{19}NO_2$, CH_4O
Formula mass	269.33	269.33	301.37
Crystal system	Orthorhombic	Monoclinic	Monoclinic
a / Å	7.963(3)	8.8254(7)	8.9139(8)
b/ Å	11.713(3)	18.3093(14)	9.1407(7)
c / Å	15.708(4)	9.0671(6)	19.7111(16)
α / °	90	90	90
β / °	90	94.273(3)	96.114(3)
γ / °	90	90	90
Unit cell volume / Å^3	1465.2(8)	1461.1(2)	1596.9(2)
Temperature / K	298	150(2)	150(2)
Space group	$P2_12_12_1$	$P2_1$/c	$P2_1$/c
No. of formula units per cell, *Z*	4	4	4
No. of reflections measured	-	107936	101718
No. of independent reflections	1611	5612	6125
R_{int}	-	0.0624	0.0327
Final R_1 values ($I > 2\sigma(I)$)	0.0499	0.0495	0.0410
Final w$R(F^2)$ values ($I > 2\sigma(I)$)	0.1316	0.1264	0.0503
Final R_1 values (all data)	-	0.0756	0.1150
Final w$R(F^2)$ values (all data)	-	0.1412	0.1222
Goodness of fit on F^2	1.125	1.024	1.060

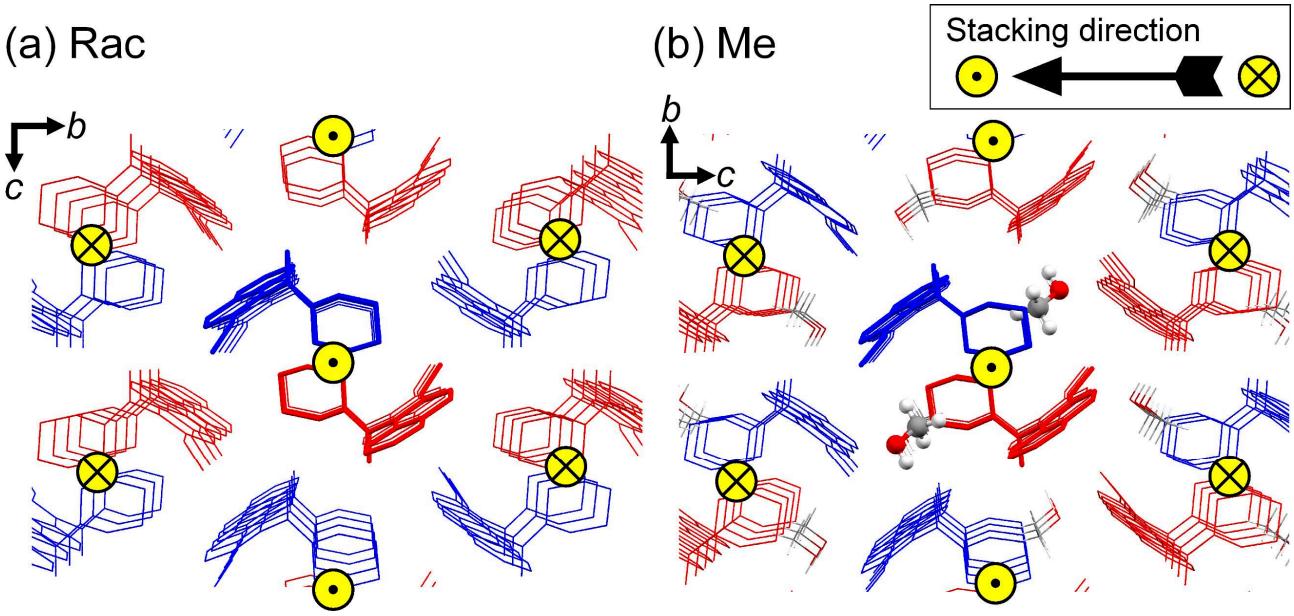

Figure 4.5 Crystal packing of (a) Rac and (b) Me along the a-axis. Hydrogen atoms are omitted for clarity. The R- and S-isomers are shown in red and blue, respectively.

In Rac, the centrosymmetric pairs are stacked along the *a*-axis. Other columns with the same stacking direction are arranged in an *ac* plan, and columns with opposite stacking directions are arranged in the next *ac* plane shifted by + and − 1/2 along the *b*-axis (Figure 4.5a). In Me, the packing structure is basically the same as that in Rac (Figure 4.5b). However, the differences between the Rac and Me packing structures are as follows: (i) the MeOH molecules are accommodated in the pocket next to the molecules of **4** and (ii) the stacking direction of the columns in the adjacent *ab* plane is the same but with the centrosymmetric pairs swapped.

The intermolecular interactions were analyzed using the short contact function incorporated in Mercury software (version 4.10). Figure 4.6 depicts the patterns of the intermolecular interactions in Rac and Me. Table 4.4 and Table 4.5 show the interaction motifs and their parameters. Hirshfeld surface analysis (Figure 4.7), a useful tool for evaluating the most dominant intermolecular interactions in crystals, was performed with CrystalExplorer software (version 17.5).

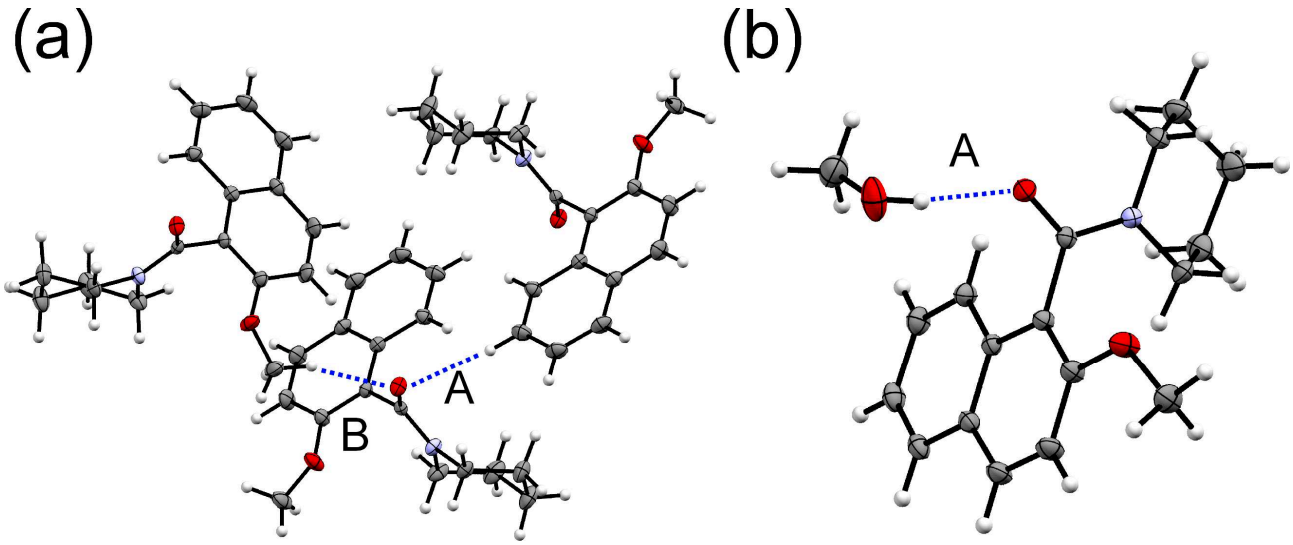

Figure 4.6 Patterns of intermolecular interactions in (a) Rac and (b) Me.

Table 4.4 Intermolecular interactions and the length and angle in Rac.

Pattern	Interaction motif	DH···A (Å)	∠DHA (°)
A	CH/O	3.529(1)	172.2
B	CH/O	3.316(1)	149.3

Table 4.5 Intermolecular interactions and the length and angle in Me.

Pattern	Interaction motif	DH···A (Å)	∠DHA (°)
A	CH/O	2.757(1)	171(2)

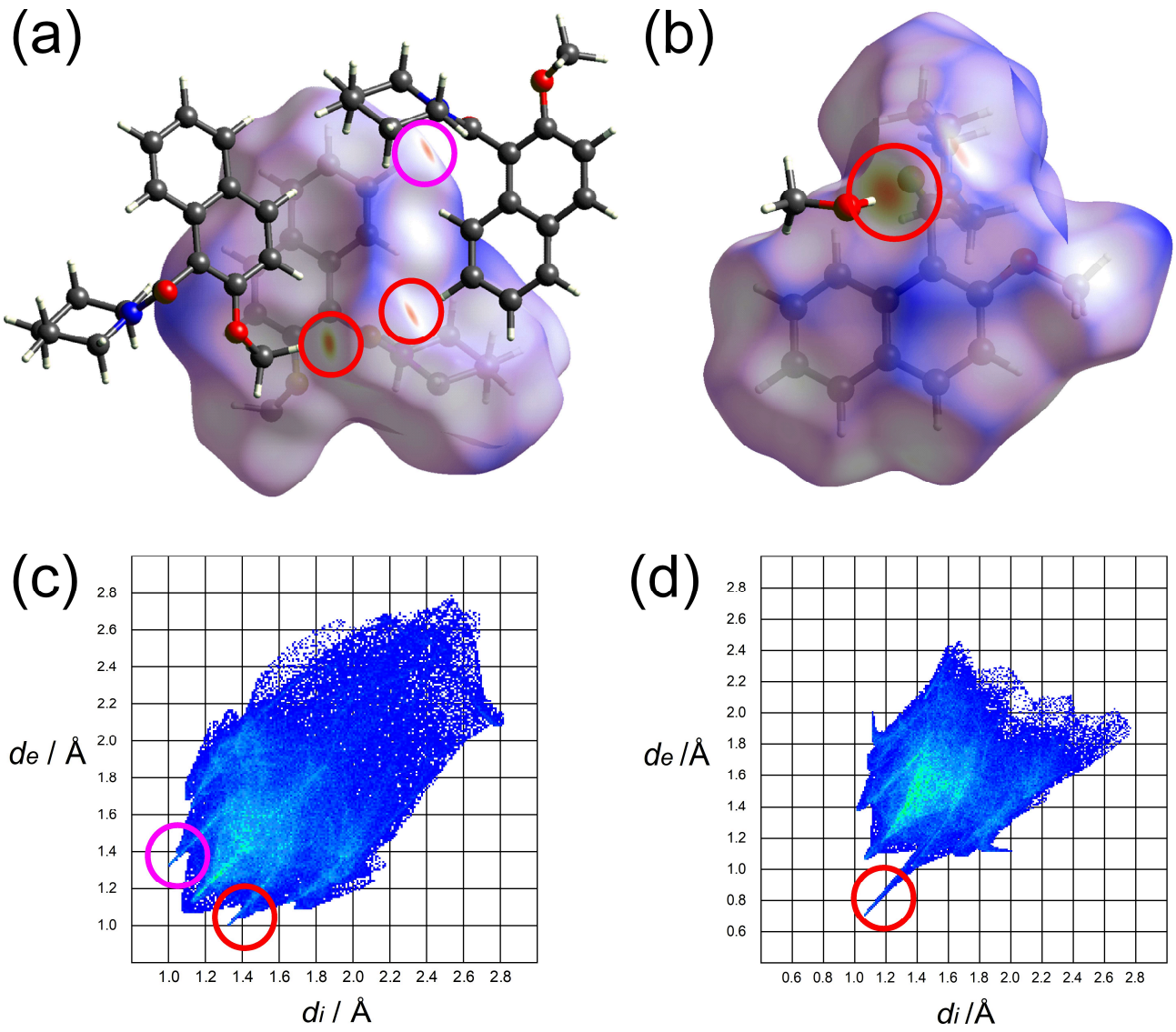

Figure 4.7 (a), (b) Hirshfeld surface of 1 in the asymmetric unit with an adjacent molecule(s), and (c), (d) the corresponding fingerprint plots of Rac (left) and Me (right).

4.3 Racemization behavior

To confirm the racemization of **4** in solution and to implement deracemization by SOAT, the kinetic constants, k_1, for the racemization process were measured by the following procedure. The racemization rate constants (k_1 values) of **4** in MTBE, MIBK, tBuOH, iPrCN, and MeOH were determined by time-course measurements of optical rotation at 365 nm using a polarimeter (MCP 5100, Anton Paar). The temperature of the sample cell (3 × 100 mm, Ni alloy) was controlled at 15, 20, 25, 30, 35, and 40 °C (±0.1 °C). The measurements were taken at 15-60 s intervals. The racemization kinetic constants were evaluated with first-order kinetics, and the slope of $\ln[\alpha_t/\alpha_0]$ as a function of time was used to determine k_1 in a manner similar to that in the previous report. The values of k_1 and temperature were used to construct an Arrhenius plot to determine the Gibbs free energy of activation ($\Delta G^{\ddagger}$), which was determined to be 96 kJ·mol^{-1}. The details are summarized in Table 4.6.

Table 4.6 Summary of the racemization kinetic constants ($k_1/10^3 \cdot s^{-1}$), half-life time ($t_{1/2}$/min), and the Gibbs free energy of activation ($\Delta G^{\ddagger}$ / kJ·mol^{-1}) of 4.

Temp. / °C	MTBE		MIBK		iPrCN		tBuOH		MeOH		MeOH/H_2O (7/3, v/v)	
	k_1	$t_{1/2}$	k_1	$t_{1/2}$	k_1	$t_{1/2}$	k_1	$t_{1/2}$	k_1	$t_{1/2}$	k_1	$t_{1/2}$
15	0.95	12.2	0.46	25.2	-	-	-	-	-	-	-	-
20	1.76	6.6	0.85	13.5	0.35	33.0	-	-	0.03	367.3	-	-
25	3.16	3.7	1.44	8.0	0.62	18.6	0.18	64.9	-	-	-	-
30	5.01	2.3	2.64	4.4	1.09	10.6	0.34	34.2	0.11	105.6	0.06	205.7
35	-	-	-	-	2.07	5.6	0.60	19.4	0.21	55.5	0.10	114.3
40	-	-	-	-	-	-	1.10	10.5	0.36	32.1	0.19	61.7
45	-	-	-	-	-	-	-	-	-	-	0.34	34.2
$\Delta G^{\ddagger}$	81.2		83.9		88.5		93.8		93.4		96.2	

The racemization rate was slower in polar solvents than in nonpolar solvents, particularly in protic solvents such as MeOH and a mixture of MeOH/H_2O (70/30, v/v). This behavior is similar to that of pyrrolidine derivative **1**, and these observations can be attributed to hydrogen bonding between the carbonyl oxygen atom of **4** and the solvent, which reduces the rate of racemization.

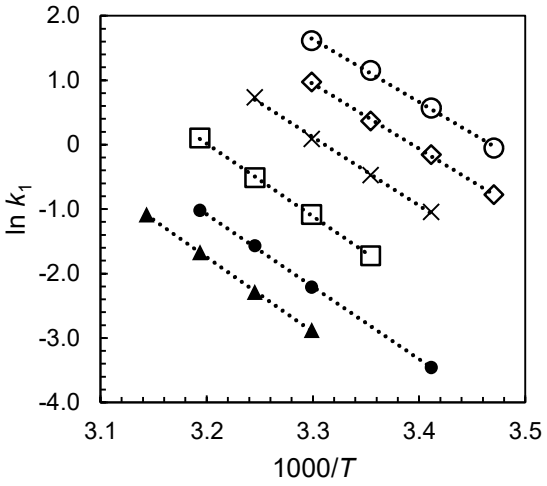

Figure 4.8 Arrhenius plot for the racemization rate of 4 in MTBE (○), MIBK (◇), iPrCN (×), tBuOH (□), MeOH (●), and MeOH/H_2O (7/3, v/v) (▲).

4.4 Quaternary phase diagram

Since the quaternary equilibria of MeOH, H_2O, and the enantiomers of **4** resulted in a complicated system due to spontaneous racemization in solution, we briefly introduce the ternary systems of the chiral molecule corresponding to the solid phases of **4**. Figure 4.9 summarizes the ternary phase diagrams of the enantiomers of a chiral molecule with a solvent and the diagrams in which the enantiomers are racemizable in solution.[117–120] Any mixture in the undersaturated or saturated solutions will shift toward a racemic composition because of racemization in the liquid phase. Many studies have reported the irreversible shift toward a single enantiomer in the solid-state with a racemizable conglomerate-forming system.[8,10,45,80,121] As long as the solution phase of the system remains undersaturated, the enantiomeric excess of the system will remain at zero. However, once the conglomerate starts to crystallize, the system must consist of a racemic solution and an enantiomerically pure solid. In the case of a racemic compound, only a racemic suspension and a racemic solution are accessible to the system in equilibrium.

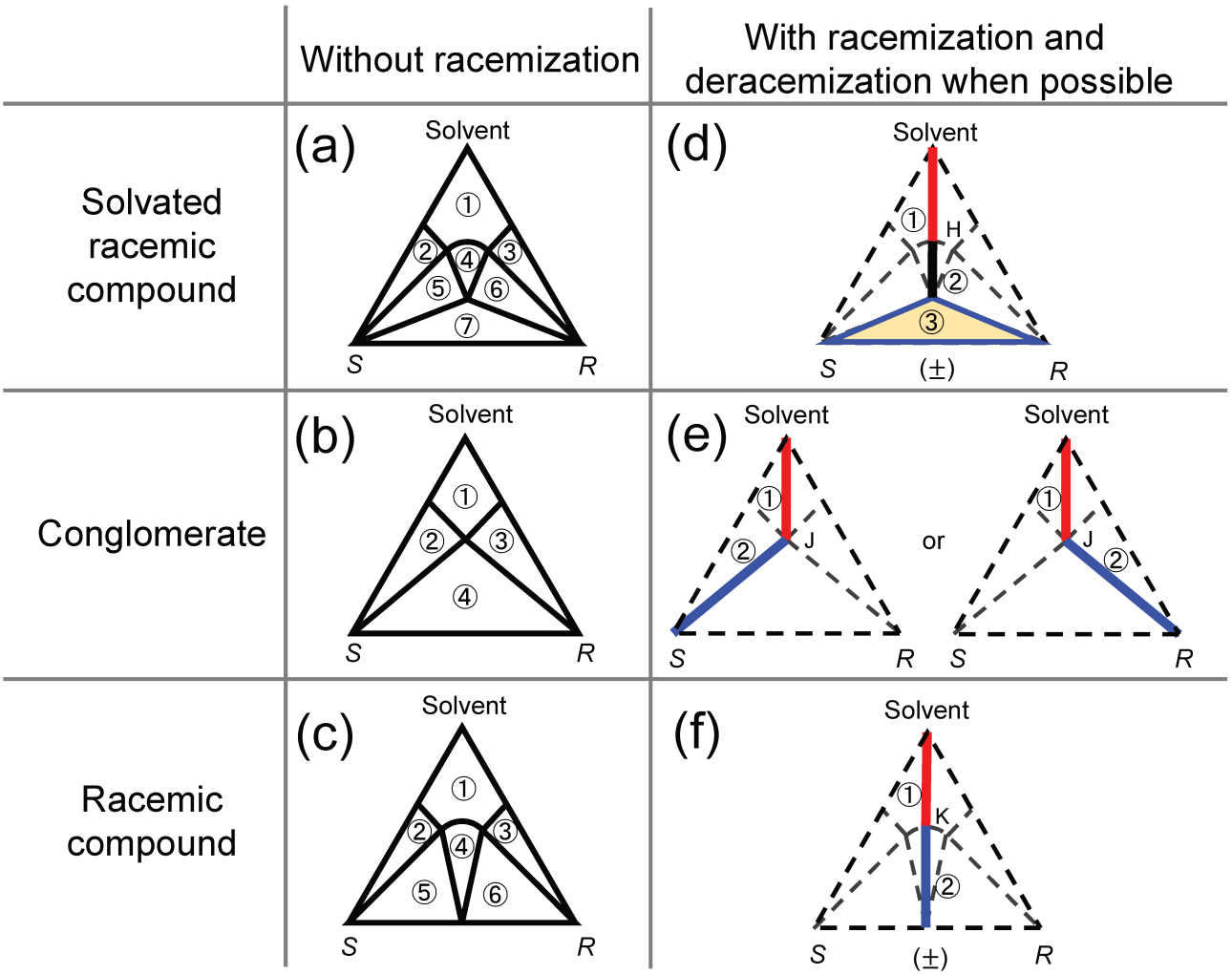

Figure 4.9 Ternary system of a solvated racemic compound, a conglomerate, and a racemic compound and the corresponding degenerate system due to racemization in solution. Only domains bound by solid lines are accessible. *Deracemization is supposed to occur only when a stable conglomerate is in contact with a solution.* The stable phases for the ternary system are: (a) ① undersaturated solution, ② ⟨S⟩+ saturated solution, ③ ⟨R⟩+ saturated solution, ④ ⟨(±)·MeOH⟩ + saturated solution, ⑤ ⟨(±)·MeOH⟩+⟨S⟩+ saturated solution, ⑥ ⟨(±)·MeOH⟩ + ⟨R⟩+ saturated solution, and ⑦ ⟨(±)·MeOH⟩+⟨S⟩+⟨R⟩; (b) ① undersaturated solution, ② ⟨S⟩+ saturated solution, ③ ⟨R⟩+ saturated solution, and ④ ⟨S⟩ + ⟨R⟩ + racemic saturated solution; and (c) ① undersaturated solution, ② ⟨S⟩ + saturated solution, ③ ⟨R⟩ + saturated solution, ④ ⟨(±)⟩ + saturated solution, ⑤ ⟨S⟩ + ⟨(±)⟩ + doubly saturated solution, and ⑥ ⟨R⟩ + ⟨(±)⟩ + doubly saturated solution. The stable phases for the degenerate ternary equilibrium are (d) ① undersaturated solution, ② ⟨(±)·MeOH⟩+ racemic saturated solution H, and ③ ⟨(±)·MeOH⟩+⟨S⟩+⟨R⟩; (e) ① undersaturated solution or ② ⟨S⟩ or ⟨R⟩ + racemic saturated solution J; and (f) ① undersaturated solution and ② ⟨(±)⟩ + racemic saturated solution K.

Figure 4.10 shows a schematic of the isothermal and isobaric quaternary system of MeOH, H_2O, and the enantiomers of **4**. Every face of the tetrahedron represents a ternary isotherm. Compound **4** forms a stable MeOH-solvated racemic compound in methanol. Compound **4** also forms a stable conglomerate in water. Because compound **4** undergoes spontaneous racemization in any solution, these two isotherms are degenerate. Regarding the racemic isoplethal section outlined in yellow lines, (±)-**4**/MeOH/H_2O, two cases were observed depending on the temperature, as shown in Figure 4.11.

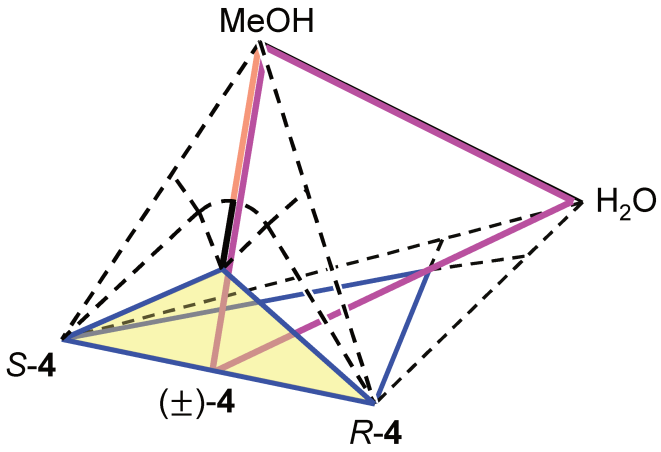

Figure 4.10 Quaternary isotherm system with the two enantiomers of 4, MeOH, and H_2O. The triangular face (MeOH/*S*-4/*R*-4) represents the ternary isotherm, indicating a stable solvated racemic compound that undergoes racemization. The base of the tetrahedron corresponds to the ternary isotherm (H_2O/*S*-4/*R*-4) showing the stable conglomerate with racemization. The magenta triangular plane is the racemic isoplethal section, (±)-4/MeOH/H_2O.

Depending on the solvent composition, the solid phases C, Rac, and Me could be stable in the racemic isoplethal section, with Me being the most stable phase at a high MeOH concentration, Rac being the most stable phase at a moderate MeOH concentration, and C being the most stable phases at low MeOH concentrations. Surprisingly, regardless of the relative stability of C with Rac in the binary system, Rac is a more stable phase than C at a moderate MeOH concentration at lower temperatures. Indeed, C crystals were converted to Rac in such a suspension, and cross-seeding experiments gave the same results. Point H indicates the solubility of Me in MeOH. Point I is the common point in the solubility curves of Me and Rac. In this case, these two phases would have monotropic character, and

point I' would not exist in equilibrium. At point I', the intersection of the solubility curves of Rac and C, the three solid phases coexist before racemization occurs. Thus, measuring the point where the composition of the two phases do not change is a straightforward approach for confirming the existence of I'. We used XRPD measurements after cross-seeding and continuous stirring for one week to confirm the presence of point I'.

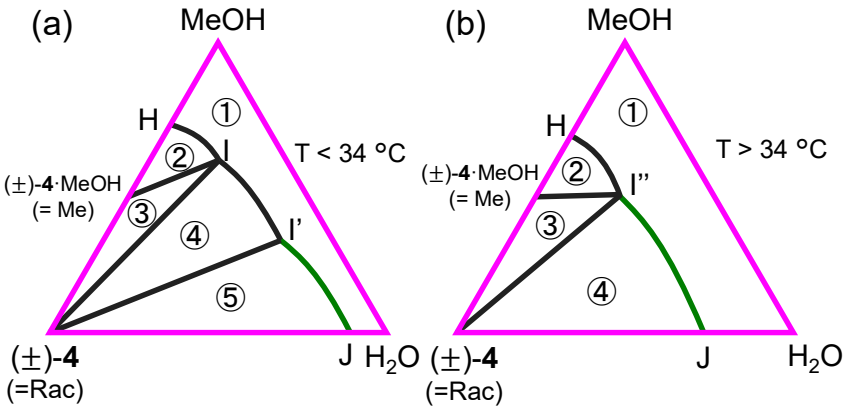

Figure 4.11 The ternary equilibrium at the racemic isoplethal section of (±)-4/MeOH/H_2O (a) below 34 °C ① unsaturated solution, ② ⟨(±)-4·MeOH⟩ + saturated solution, ③ ⟨(±)-4⟩ + ⟨(±)-4·MeOH⟩ doubly saturated solution I, ④ ⟨(±)-4⟩ + saturated solution, and ⑤ ⟨(+)-4⟩ + ⟨(−)-4⟩ + saturated solution and (b) above 34 °C ①unsaturated solution, ② ⟨(±)-4·MeOH⟩ + saturated solution, ③ ⟨(+)-4⟩ + ⟨(−)-4⟩ + ⟨(±)-4·MeOH⟩ triply saturated solution I", and ④ ⟨(+)-4⟩ + ⟨(−)-4⟩+ saturated solution. Every solution was racemic.

Figure 4.12 summarizes the isothermal and isobaric quaternary systems with and without racemization. The domains highlighted in green or purple represent the areas of chiral discrimination, i.e., these domains involve conglomerates. Another similar case was described in detail in a review.[122] Under the usual conditions (without racemization) of Case 1, the upper surface of the conglomerate stability domain is delineated by the *S* – *R* – I' plane, which contains the racemic compound (±). In Case 2 without deracemization, the two symmetrical quadriphasic domains related to the racemic plane are delineated by the line from the common point I'' to the stoichiometric point of (±)-**4**·MeOH. Beyond point I'', as the concentration in water increased, there was a single monovarient curve down to the doubly saturated solubility point (J) in pure H_2O, which represents

the edge of the stable conglomerate domain. Conversely, in the case of the deracemization of the conglomerate, the crystals of a single enantiomer and a racemic solution are in equilibrium at the end of the deracemization, as described above. Thus, both cases are degenerate and can be considered based on the system shown in the right column of Figure 4.12.

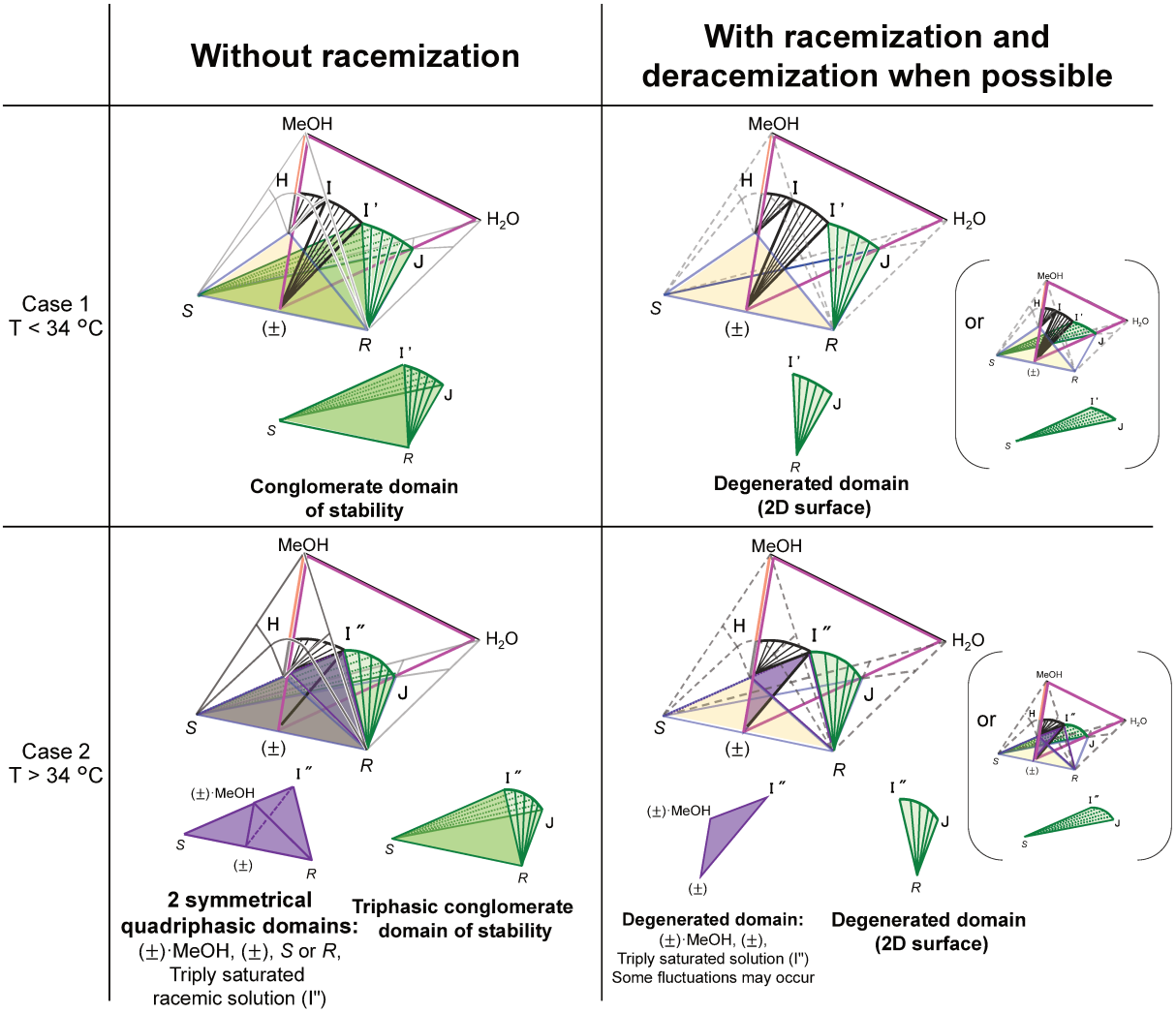

Figure 4.12 Quaternary system with two different solvents (MeOH and H_2O) and two enantiomers (*R* and *S*) with and without racemization in the liquid phase with the two types of racemic isoplethal sections shown in Figure 4.11. The systems that involved racemization correspond to (±)-4/MeOH/H_2O. In Case 1, the curves in the racemic isoplethal section (H – I, I – I', I' – J) correspond to the solubility curves of Me, Rac, and C, respectively. When deracemization occurs, the stable conglomerate domain degenerates to a 2D surface involving one of the enantiomers and the racemate (±), as colored in green. In addition, the domain in the ternary system (MeOH/*R*/*S*) is also involved in the equilibrium. In Case 2, the solubility lines in the racemic isoplethal section (H – I" and I" – J) correspond to the solubility curves of Me and C, respectively. In contrast to Case 1, the stable conglomerate domain does not include the racemate (±). Only domains bound by solid lines are accessible.

To understand the concrete heterogeneous equilibrium at different temperatures, we studied the isoplethal sections of (±)-**4**/MeOH/H_2O at 15, 20, 23, 28, and 34 °C. The solubilities of **4** in MeOH and in the mixture of MeOH and H_2O were measured in triplicate using a gravimetric method or by the determination of a clear point using Crystal16 (Technobis B.V.). The identity of the solid phase(s) in equilibrium with a saturated solution was monitored by XRPD analysis. To ensure the stability of the solid phase in a solution with a specific composition, the sample for the solubility measurement was prepared by a cross-seeding technique, i.e., a mixture of crystals of different forms was added to the clear saturated solution at the given temperature and a long period was allowed elapse before sampling the solution and analysis of the solid phases by XRPD.

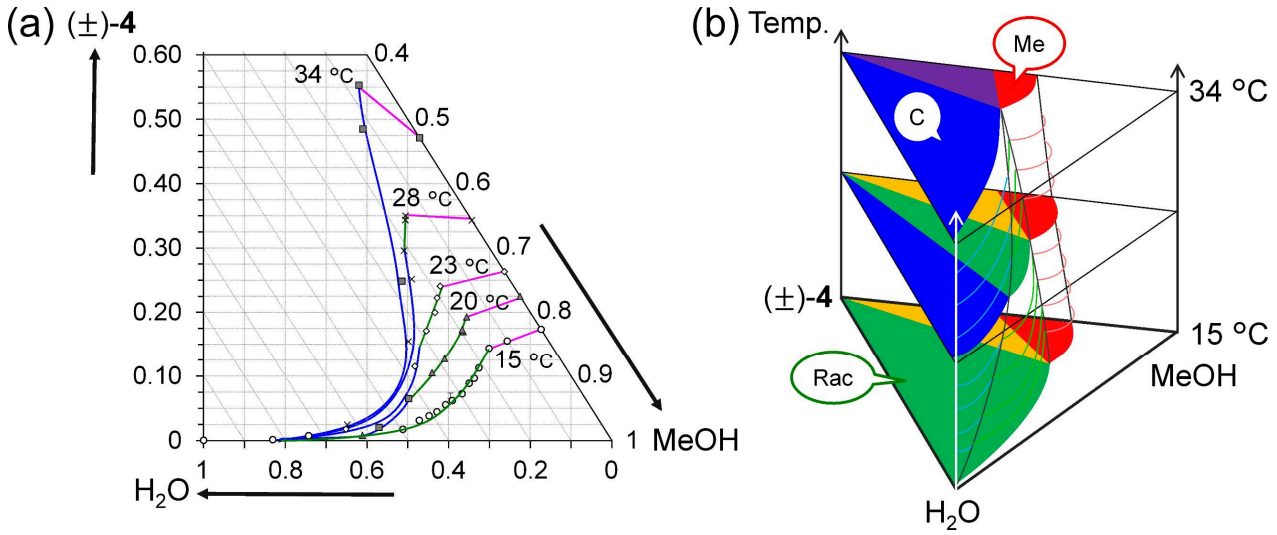

Figure 4.13 (a) The isoplethal sections of the quaternary phase diagrams of the (R)- and (S)-enantiomers of 4, H_2O, and MeOH at 15 °C (○), 20 °C (▲), 23 °C (◇), 28 °C (×), and 34 °C (■). (b) Schematic of the isoplethal section along the temperature axis.

Interestingly, under ambient conditions, Rac has a large stability domain at 15 °C at high water concentrations, as seen in Figure 4.13. Furthermore, the stable C domain gradually expands at higher temperatures. Point I' exists at relatively high concentrations of H_2O at low temperatures and shifts toward lower concentrations of H_2O at higher temperatures. While the size of the domain for Me does not change significantly, point I remains at almost the same composition. As a result, points I' and I merge into I'' at 34 °C, and the domain of stable Rac disappears, indicating that Rac is no longer

stable above 34 °C. Because Me is desolvated at 50 °C and cannot exist above this temperature, the size of the domain of stable C expands in a two-step manner up to 50 °C.

Overall, this thorough phase diagram study affords guidelines for the chiral separation of **4** by crystallization. As a conglomerate-forming system is necessary, the chiral separation could be ideally implemented above 34 °C. Considering the solubility of **4**, the chiral separation of **4** was carried out in MeOH/H_2O (70/30, v/v) above 28 °C, and at this solvent composition, C is stable, and its solubility is moderate at this operating temperature.

4.5 Deracemization by SOAT

Generally, a slow racemization of the molecule during the deracemization process is not preferable because the enantiomeric composition in the solution during the crystallization gradually shifts in the direction of the undesired enantiomer, which could eventually cause nucleation of the undesired enantiomer due to the relatively high supersaturation, as shown in Figure 4.14.

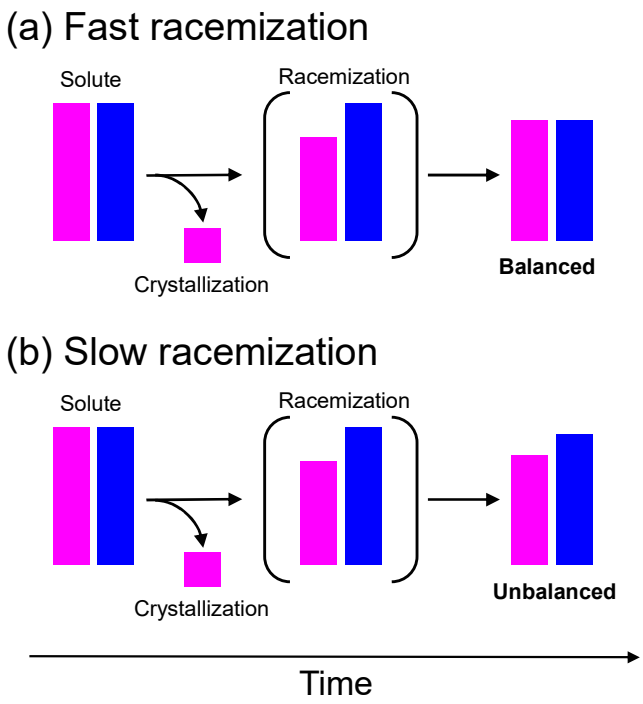

Figure 4.14 Schematic representation of the chiral separation by crystallization with (a) fast racemization and (b) slow racemization.

In this context, the deracemization of **4** in a mixture of MeOH/H_2O (70/30, v/v) would not be preferable. Further screening tests might provide a solution to such problematic cases. However, considering the feasibility of SOAT, solubilities that are too high or too low can cause problems in different MeOH mixtures. Thus, we used a mixture of MeOH and H_2O and optimized the crystallization duration because the behavior of **4** had been well studied in this system, as mentioned above.

The SOAT of **4** was carried out according to the following procedure. To a double-jacketed, 100-mL crystallizer (Reactor-Ready Lab reactor, Radleys) equipped with a thermocouple and a mechanical stirrer were added compound **4** and MeOH/H_2O (70/30, v/v), and the mixture was heated to 50 °C with stirring (500 rpm) to completely dissolve **4**. The jacket temperature was controlled using a thermostat (Unichiller, HUBER). The solution was cooled to 34 °C at a rate of 1 $K \cdot min^{-1}$, and the temperature was maintained for 20 min. The seed crystals (>99% *ee* of the *R* or *S* isomer) were added to the solution at a stirring rate of 200 rpm, and the solution was cooled to 28 °C with a controlled cooling profile. Typically, the optimization of cooling curves for different operating conditions is complex. However, Mullin *et al.* reported the simplified relationship depicted by Eq. (1), which is adequate for general applications.[123]

$$\theta_t = \theta_0 - (\theta_0 - \theta_f)\,(t/\tau)^3 \qquad \text{(Eq. 1)}$$

Here, θ_0, θ_f, and θ_t are the temperatures at the beginning, end, and any time t during the crystallization, respectively, and τ is the overall duration of the crystallization. The details of the operating conditions are summarized in Table 4.7.

Table 4.7 Operating conditions for the SOAT of 4

Mass of **4** (g)	28.2
Mass of solvent (g)	85.4
Concentration (wt%)	24.8
Mass of seeds (g)	1.00
Stirring speed (rpm)	200
Duration (h)	10, 15, 20

The accurate chiral composition of **4** in the solid samples (powder or single crystals) was determined using high-performance liquid chromatography (HPLC) with an (*S*,*S*) Whelk-O1 column (Regis Technologies, Inc., ⌀4.6 × 250 mm× 5 μm), employing a mixture of heptane and isopropyl alcohol (1/1, v/v) as the mobile phase at a flow rate of 1.5 mL/min. The wavelength employed for UV detection was 230 nm. To suppress racemization during analysis, the column temperature was controlled at 0 °C using a thermostat with a double glass jacket. Under these conditions, retention times of 3.8 and 5.5 min were observed for (*R*)-**4** and (*S*)-**4**, respectively. The analyses were performed using a SpectraSYSTEM (P1000XR, AS3000, UV2000, and SN4000, and Fisher Thermo Scientific). The enantiomeric excesses (*ee*s) were obtained by integrating and comparing the peak areas of (*R*)-**4** and (*S*)-**4** using ChromQuest software.

The results of the SOAT of **4** are summarized in Table 4.8. As expected from the racemization behavior of **4**, the short crystallization duration of 10 h resulted in the isolated crystals having a low *ee*. A crystallization duration of 20 h furnished a high *ee* with a maximum of 97% *ee*. To confirm the reproducibility of the experiment, we performed the SOAT with the same duration and used seed crystals of the opposite enantiomer, which afforded a good *ee* after 20 h with an average value of 90% *ee*. The average volumetric productivity,[75] which indicates the quantity of the desired product that can be obtained per unit time and volume, for the process was 6.5 g h^{-1} L^{-1}. Compared to our previous

study,[14] which compared the productivities of SOAT and TCID, the productivity in the present work is low owing to the long crystallization duration required by the poor racemization rate.

Table 4.8 Experimental results of the SOAT of 4 in MeOH/H_2O (70/30, v/v).

Duration / h	m_{crop} / g	ee_{final} [%]	Productivity / g h^{-1} L^{-1}
10	16.5	(*S*) 11	0.9
15	14.7	(*S*) 68	6.0
20	16.1	(*S*) 97	7.3
20	15.4	(*R*) 92	6.6
20	14.9	(*R*) 81	5.5

4.6 Conclusion

The crystal structures of Rac and Me axially chiral naphthamide **4** have been determined. A quaternary phase diagram of the enantiomers of **4** in MeOH and H_2O was constructed. In particular, the impact of temperature on the racemic isoplethal section of **4** in solution was thoroughly studied over a temperature range from 15 to 34 °C. At 15 °C, Rac is stable at high H_2O concentrations, while Me is stable at low H_2O concentrations. The domain of stable C gradually expands from a high H_2O concentration region with increasing temperature. At 34 °C, the domain for Rac disappears, and only C and Me are stable up to 50 °C. The phase diagram study confirmed that the chiral separation of the enantiomers of **4** by SOAT in MeOH/H_2O (70/30, v/v) resulted in crystals with high enantiopurity (up to 97% *ee*). These results further prove the efficiency of the phase diagram approach for enabling chiral separation by crystallization even when the compound can form a stable racemic compound, which is typically challenging. The lessons from the present study will serve as a model for developing deracemization applications for industrial processes.

General conclusion & Discussion

This Ph.D. work is dedicated to elucidating deracemization by experimental approaches using atropisomers that are racemizable in solution yet exhibit frozen chirality in the crystalline state.

In Chapter 2, we focused on the role of racemization kinetics on TCID. To clarify its impact, we chose an atropisomeric naphthamide derivative that forms a stable conglomerate and exhibits spontaneous racemization in solution. The racemization kinetics were characterized by first-order kinetic constants, k_1, in several solvents such as alcohols, ethers, ketones, and nitriles, and it was found that k_1 varies by 2 orders of magnitude depending on the type of solvent. For example, in alcohols, racemization is almost 50 times slower than in ethers. TCID experiments were carried out in four solvents, an ether, an alcohol, a ketone, and a nitrile. For practical reasons, the global deracemization rate was evaluated based on the time required to reach 90% *ee* from 10% *ee*. The TCID and racemization kinetics studies showed that the logarithm of the racemization rate is linearly correlated with the global deracemization rate. In addition, the process productivity of TCID is also correlated with the product of solubility and k_1.

In Chapter 3, we compared the process productivity of TCID and SOAT using the same molecule as used in Chapter 2 because we noticed that the process productivity of TCID was lower than those of classic techniques such as PC. To keep the conditions as constant as possible, we chose an azeotropic mixture of ethyl acetate and cyclohexane. Naphthamide derivatives have good solubility and fast racemization kinetics in such solutions. Interestingly, the process productivity of TCID is almost independent of the scale of the deracemization. Of course, a much larger scale can influence the efficiency of stirring and heat exchange, so process productivity will not be independent of the scale of production. Although TCID gave crystals with a high purity (>99% *ee*), the productivity of SOAT was 100 times greater. Moreover, SOAT can easily be scaled up; a 10-g scale process gave almost the same result as the 1-g scale process. These results suggest that TCID and SOAT can be used properly depending on the purpose. For instance, TCID can be a good choice for producing enantiopure

crystals when there are no enantiomerically pure crystals available. On the other hand, SOAT is productive and easily scaled up, making it suitable for production.

In Chapter 4, we investigated the SOAT of an atropisomeric naphthamide derivative that exhibits three solid phases using a phase diagram study. To separate compounds that show multiple phases, such as those that show polymorphism, it is important to understand the behavior of each phase. A phase diagram gives the land scape of the solid-phase behavior and is useful for designing a crystallization path; however, the number of reports regarding deracemization is limited, which may be because racemization adds complexity to phase diagrams. Indeed, a phase diagram of a racemizable compound results in a degenerate system. Hence, we developed a phase diagram for deracemization to provide an experimental example that can facilitate designing a separation and crystallization process. To construct a quaternary phase diagram, we measured the solubility of the naphthamide derivative in a mixture of methanol and water and determined the stable phase. According to the phase diagram study, the compound forms a stable conglomerate in a water-rich solution. Based on the phase diagram, we carried out the SOAT of the naphthamide derivative and achieved deracemization up to 97% *ee*. These results provide the first example of a phase diagram enabling a deracemization, which will facilitate the industrial application of SOAT.

Since the first experimental demonstration of symmetry breaking by Kondepudi, many researchers have investigated deracemization, and its application to industry may be imminent. Particularly, the applicability of deracemization for many compounds has been actively studied in the most recent 10 years. The next challenges in this field to be addressed before industrial application include understanding the mechanisms behind deracemization for safety and robust operation. In this context, this Ph.D. work contributes to providing a guideline for estimating deracemization behaviors using model compounds from a practical and fundamental approach, as summarized above. Chapters 2 and 3 are devoted to providing practical information. In Chapter 2, the impact of racemization kinetics has been quantitatively clarified, which implies that the global deracemization rate can be easily estimated by measuring the racemization rate and the solubility. In Chapter 3, the performances of

deracemization by TCID and SOAT are compared, and the advantages of each technique are revealed. The conclusions from these chapters are practically useful information for the preliminary stage of process design. By contrast, in Chapter 4, a phase diagram study, which is a fundamental topic of crystallization, is considered for successful deracemization. Because of the racemization in the solution, the construction of a phase diagram was lacking in technology used in the study of deracemization. To promote the usefulness of phase diagrams, we have reported these results in a didactic way, i.e., including how to construct and use the phase diagram for deracemization. Animated movie is available in the supporting information of the publication (DOI: 10.1002/chem.201903338). Although this thesis can be a milestone for promoting our understanding of the practical and fundamental aspects of deracemization, further investigations to expand its applicability from various aspects are needed. First, the generality of the conclusions in all chapters must be verified in different environments since the model compounds exhibit simple racemization kinetics, while most compounds do not. Recently, the group of Mazzotti investigated the role of racemization kinetics in deracemization using NMPA and DBU, which follow second-order reaction kinetics, and reached similar conclusions as those in Chapter 2.[124] Further reports supporting the conclusions in this thesis are needed. Second, a reliable method to control the resulting chirality in deracemization is necessary for industrial applications. We have not paid attention to the chirality of the crystals after deracemization, since this work is dedicated to extracting the information behind deracemization, but a single enantiomer is demanded when we perform a chiral separation. Thus, obtaining the desired enantiomer is very important, as is a productive deracemization process. Vlieg and coworkers reported the impact of chiral impurity on controlling the chirality of crystals resulting from deracemization.[13] In this work, the nucleation of undesired enantiomers is inhibited by impurities that promote the crystallization of the desired enantiomer. The main point in controlling the chirality is reducing the amount of external chiral sources. These two points are not studied in this work but are demanded for the industrial application of deracemization.

Experimental details

Synthesis and preparation of naphthamide

To a mixture of K_2CO_3 (553 g, 4.00 mol, 3.00 equiv) and 2-hydroxy-1-naphthoic acid (**2**, 250 g, 1.33 mol, 1.00 equiv) in acetone (1.2 L) was added dimethyl sulfate (255 mL, 2.69 mol, 2.02 equiv) dropwise at 10 °C, and the reaction mixture was stirred with a mechanical stirrer at 50 °C for 3 h. The precipitate was then removed by filtration, and the solvent was evaporated under reduced pressure. The residue was dissolved in diethyl ether (1 L) and washed with sat. aq. $NaHCO_3$ (500 mL × 2). The organic layer was concentrated under reduced pressure to give a pale-yellow liquid. The obtained crude material was then treated with 2 M NaOH (500 mL) in EtOH (500 mL) under reflux for 16 h. The solvent was evaporated under reduced pressure, and the residue was dissolved in H_2O (1.2 L) and washed with ethyl acetate (500 mL × 2). The aqueous layer was acidified to pH = 1 with conc. HCl, and the precipitate was collected by filtration and dissolved in ethyl acetate (1 L). The organic layer was washed with brine (300 mL) and dried over $MgSO_4$, and the solvent was evaporated under reduced pressure to give pale yellow crystals of 2-methoxy-1-naphthoic acid (**3**, 250 g, 93%, 2 steps). Although the color of the crude material could be removed by treatment with activated carbon, it was sufficiently pure for use in the following reaction.

To a solution of **3** (1.36 g, 6.73 mmol, 1.0 equiv) in tetrahydrofuran (THF) (50 mL) at 0 °C was added thionyl chloride (0.6 mL, 8.3 mmol, 1.2 equiv), and the mixture was stirred for 30 min. Pyrrolidine (1.65 mL, 20 mmol, 3.0 equiv) was then added dropwise to the reaction mixture, after which it was stirred for an additional 3 h. The solvent was then evaporated under reduced pressure, and the crude material was dissolved in ethyl acetate (100 mL) and washed with sat. aqueous $NaHCO_3$ (100 mL × 2). The organic layer was dried over $MgSO_4$, and the solvent was evaporated under reduced pressure. The residue was purified by silica gel column chromatography (CH_2Cl_2/EtOAc, 1/1, v/v) to yield a pale yellow solid. The solid was recrystallized from a mixture of CH_2Cl_2/heptane (1/1, v/v) to give colorless crystals of **1** (1.49 g, 88%). Large single crystals (5–30 mg) for racemization rate experiments were prepared by the slow evaporation of a saturated 1:1 (v/v) $CHCl_3$:heptane solution.

Temperature cycle-induced deracemization (TCID)

TCID experiments involving **1** were carried out by temperature cycling of the saturated solution in equilibrium with the crystals, as described in the following procedure. First, compound **1** was completely dissolved at 50–60 °C in the required solvent in a 40-mL screw vial, and the solution was filtered through a membrane filter. The filtered solution was maintained at 20 °C until crystallization spontaneously occurred. The first crystals are usually slightly (< 3%) enriched with one enantiomer at random. Temperature cycling, shown in Figure ex1, was then performed between 20 and 25 °C for 5–7 d. For the off-line monitoring of the deracemization experiments involving **1**, a small amount (~50 μL) of the suspension was removed and filtered through a filter paper in a Kiriyama Rohto VB-8 funnel. The collected crystals were dried under vacuum, precisely weighed, and dissolved in MeOH (1.200 mL, HPLC grade) at 4 °C. The enantiomeric excess was determined by comparing the optical rotation at 365 nm and 4 °C with the previously determined specific optical rotation ($[\alpha]^{4}_{365}$= 662.3 (MeOH)). Since cooling from 25 to 20 °C corresponds to the crystal-growth step, this stage was conducted more slowly than the other steps to prevent unfavorable nucleation or growth. We showed in this study that the racemization of **1** occurs very slowly in cold MeOH; therefore, these conditions were selected to evaluate the optical rotation and to minimize the racemization of **1**. It should be noted that 20% of the crystals were deliberately dissolved during heating to directly compare the deracemization rates in different solvents (Figure ex1).

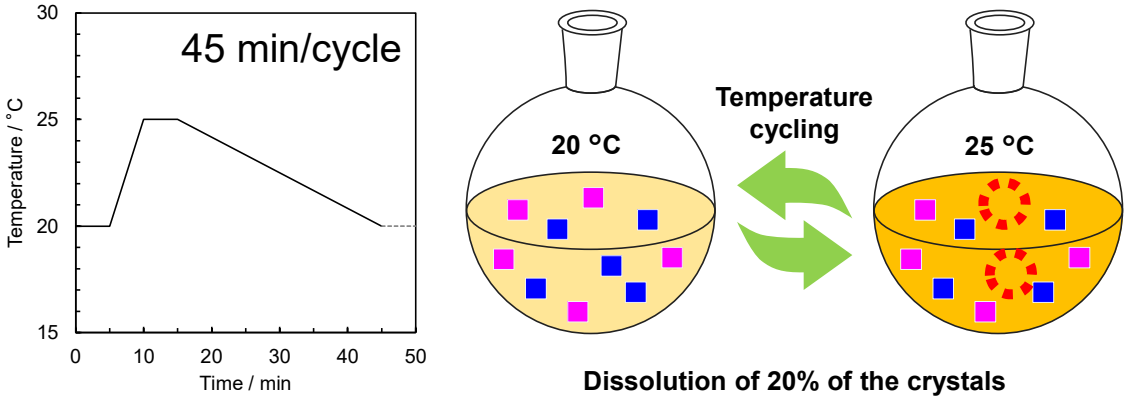

Figure ex1. Schematic illustration of the deracemization experiment and temperature profile applied in the TCID.

The solution equilibria after the heating and cooling steps were confirmed in the same manner used in the gravimetric-solubility experiments; i.e., the times for dissolution and crystal growth were suitable such that these processes were not the rate-limiting step in the experiment.

Second-order asymmetric transformation (SOAT)

A variable mass of powdered enantiopure seed crystals (prepared by grinding a single crystal) was added to a saturated solution of **1** in a 45/55 (wt/wt) mixture of cyclohexane and ethyl acetate at 60 °C (mass fraction concentration S = 22.2 wt%) in a 40-mL vial (⌀27.5 × 95 mm, VWR France, France) for the 1-g scale experiment or a double-jacketed, 150-mL three-neck flask for the 10-g scale experiment. The temperature was controlled by a thermostat (F25-HL Cryostat, JULABO GmbH, Germany). The mixture was stirred at 500 rpm by a cross-shaped magnetic stirrer throughout the experiment. After a 3-minute isotherm, the suspension was cooled to 30 °C over a period of approximately 85 min. The temperature of the solution was monitored every 30 s with a data logger (LogStick LS450-T(K), Osaka Micro Computer Inc., Osaka, Japan) connected to a thermocouple. The supersaturation of the solution was monitored during cooling by sampling aliquots of the solution for gravimetric analyses. The crystals were collected by filtration and dried under a vacuum. The enantiomeric excess was determined by comparing the optical rotation at 365 nm and 4 °C with the previously determined specific optical rotation.

References

[1] FDA's Center for Drug Evaluation and Research's (CDER's) Advancing health through innovation 2018 New drug therapy approvals, 2019.

[2] B. G. de la Torre, F. Albericio, *Molecules* **2019**, *24*, 809.

[3] P. H. Karpinski, *Chem. Eng. Technol.* **2006**, *29*, 233–237.

[4] S. L. Veinberg, K. E. Johnston, M. J. Jaroszewicz, B. M. Kispal, C. R. Mireault, T. Kobayashi, M. Pruski, R. W. Schurko, *Phys. Chem. Chem. Phys.* **2016**, *18*, 17713–17730.

[5] A. H. J. Engwerda, N. Koning, P. Tinnemans, H. Meekes, F. M. Bickelhaupt, F. P. J. T. Rutjes, E. Vlieg, *Cryst. Growth Des.* **2017**, *17*, 4454–4457.

[6] L. Spix, A. Alfring, H. Meekes, W. J. P. Van Enckevort, E. Vlieg, *Cryst. Growth Des.* **2014**, *14*, 1744–1748.

[7] L. Spix, H. Meekes, R. H. Blaauw, W. J. P. Van Enckevort, E. Vlieg, *Cryst. Growth Des.* **2012**, *12*, 5796–5799.

[8] R. R. E. Steendam, J. Dickhout, W. J. P. Van Enckevort, H. Meekes, J. Raap, F. P. J. T. Rutjes, E. Vlieg, *Cryst. Growth Des.* **2015**, *15*, 1975–1982.

[9] W. L. Noorduin, P. Van Der Asdonk, A. A. C. Bode, H. Meekes, W. J. P. Van Enckevort, E. Vlieg, B. Kaptein, M. W. Van Der Meijden, R. M. Kellogg, G. Deroover, *Org. Process Res. Dev.* **2010**, *14*, 908–911.

[10] C. Viedma, *J. Cryst. Growth* **2004**, *261*, 118–121.

[11] K. Suwannasang, A. E. Flood, C. Rougeot, G. Coquerel, *Org. Process Res. Dev.* **2017**, *21*, 623–630.

[12] R. Oketani, M. Hoquante, C. Brandel, P. Cardinael, G. Coquerel, *Cryst. Growth Des.* **2018**, *18*, 6417–6420.

[13] G. Belletti, H. Meekes, F. P. J. T. Rutjes, E. Vlieg, *Cryst. Growth Des.* **2018**, *18*, 6617–6620.

[14] R. Oketani, M. Hoquante, C. Brandel, P. Cardinael, G. Coquerel, *Org. Process Res. Dev.* **2019**, *23*, 1197–1203.

[15] J.-B. Biot, *Bull. la Société Philomath. Paris* **1815**, *1*, 190–192.

[16] L. Pasteur, *Ann. Chim. Phys.* **1848**, *24*, 442–459.

[17] R. Kuroda, S. F. Mason, *J. Chem. Soc. Dalt. Trans.* **1981**, 1268.

[18] IUPAC, *Pure Appl. Chem.* **1996**, *68*, 2193–2222.

[19] IUCr, *Acta Crystallogr. Sect. A Found. Crystallogr.* **1992**, *48*, 922–946.

[20] M. I. Aroyo, Ed. , *International Tables for Crystallography*, International Union Of Crystallography, Chester, England, **2016**.

[21] T. Hahn, H. Klapper, U. Müller, M. I. Aroyo, **2016**, pp. 720–776.

[22] J. Jacques, A. Collet, S. H. Wilen, *Enantiomers, Racemates, and Resolutions*, Wiley, **1981**.

[23] A. Berkessel, H. Gröger, *Asymmetric Organocatalysis*, Wiley, **2005**.

[24] E. García-Urdiales, I. Alfonso, V. Gotor, *Chem. Rev.* **2005**, *105*, 313–354.

[25] S. E. Denmark, J. Fu, *Chem. Rev.* **2003**, *103*, 2763–2794.

[26] T. J. Seiders, D. W. Ward, R. H. Grubbs, *Org. Lett.* **2001**, *3*, 3225–3228.

[27] F. Diederich, P. J. Stang, *Metal-Catalyzed Cross-Coupling Reactions*, Wiley-VCH, **1998**.

[28] K. Soai, T. Shibata, I. Sato, *Acc. Chem. Res.* **2000**, *33*, 382–390.

[29] J. K. Whitesell, *Chem. Rev.* **1992**, *92*, 953–964.

[30] H. U. Blaser, *Chem. Rev.* **1992**, *92*, 935–952.

[31] M. T. Gilbert, in *High Perform. Liq. Chromatogr.*, J. Wiley, **1987**, pp. 291–312.

[32] D. Kozma, *CRC Handbook of Optical Resolutions via Diastereomeric Salt Formation*, CRC Press, **2001**.

[33] J. M. Keith, J. F. Larrow, E. N. Jacobsen, *Adv. Synth. Catal.* **2001**, *343*, 5–26.

[34] H. Ito, S. Kunii, M. Sawamura, *Nat. Chem.* **2010**, *2*, 972–976.

[35] G. Coquerel, in *Top. Curr. Chem.*, **2006**, pp. 1–51.

[36] R. Tamura, D. Fujimoto, Z. Lepp, K. Misaki, H. Miura, H. Takahashi, T. Ushio, T. Nakai, K. Hirotsu, *J. Am. Chem. Soc.* **2002**, *124*, 13139–13153.

[37] F. F. Huerta, A. B. E. Minidis, J.-E. Bäckvall, *Chem. Soc. Rev.* **2001**, *30*, 321–331.

[38] L.-C. Sögütoglu, R. R. E. Steendam, H. Meekes, E. Vlieg, F. P. J. T. Rutjes, *Chem. Soc. Rev.* **2015**, *44*, 6723–6732.

[39] W. L. Noorduin, E. Vlieg, R. M. Kellogg, B. Kaptein, *Angew. Chemie Int. Ed.* **2009**, *48*, 9600–9606.

[40] K. Suwannasang, A. E. Flood, C. Rougeot, G. Coquerel, *Cryst. Growth Des.* **2013**, *13*, 3498–3504.

[41] IUPAC, *Pure Appl. Chem.* **1996**, *68*, 2193–2222.

[42] W. L. Noorduin, W. J. P. Van-enckevort, H. Meekes, B. Kaptein, R. M. Kellogg, J. C. Tully, J. M. McBride, E. Vlieg, *Angew. Chemie - Int. Ed.* **2010**, *49*, 8435–8438.

[43] D. K. Kondepudi, R. J. Kaufman, N. Singh, *Science (80-.).* **1990**, *250*, 975–976.

[44] C. Viedma, *Phys. Rev. Lett.* **2005**, *94*, 065504.

[45] W. L. Noorduin, H. Meekes, W. J. P. Van Enckevort, A. Millemaggi, M. Leeman, B. Kaptein, R. M. Kellogg, E. Vlieg, *Angew. Chemie - Int. Ed.* **2008**, *47*, 6445–6447.

[46] IUPAC, *Pure Appl. Chem.* **2007**, *79*, 1801–1829.

[47] C. Viedma, P. Cintas, *Chem. Commun.* **2011**, *47*, 12786.

[48] K. Suwannasang, A. E. Flood, C. Rougeot, G. Coquerel, *Cryst. Growth Des.* **2013**, *13*, 3498–3504.
[49] L. Guy, J. Crassous, C. Andraud, *Chirality* **2002**, *14*, 820–820.
[50] N. G. Anderson, *Org. Process Res. Dev.* **2005**, *9*, 800–813.
[51] M. Breuer, K. Ditrich, T. Habicher, B. Hauer, M. Keßeler, R. Stürmer, T. Zelinski, *Angew. Chemie - Int. Ed.* **2004**, *43*, 788–824.
[52] W. L. Noorduin, A. A. C. Bode, M. van der Meijden, H. Meekes, A. F. van Etteger, W. J. P. van Enckevort, P. C. M. Christianen, B. Kaptein, R. M. Kellogg, T. Rasing, et al., *Nat. Chem.* **2009**, *1*, 729–732.
[53] A. H. J. Engwerda, P. van Schayik, H. Jagtenberg, H. Meekes, F. P. J. T. Rutjes, E. Vlieg, *Cryst. Growth Des.* **2017**, *17*, 5583–5585.
[54] C. Rougeot, F. Guillen, J. C. Plaquevent, G. Coquerel, *Cryst. Growth Des.* **2015**, *15*, 2151–2155.
[55] M. Iggland, M. P. Fernández-Ronco, R. Senn, J. Kluge, M. Mazzotti, *Chem. Eng. Sci.* **2014**, *111*, 106–111.
[56] K. Suwannasang, A. E. Flood, G. Coquerel, *Cryst. Growth Des.* **2016**, *16*, 6461–6467.
[57] F. Brevegliери, G. M. Maggioni, M. Mazzotti, *Cryst. Growth Des.* **2018**, *18*, 1873–1881.
[58] R. Kacker, M. Radoiu, H. J. M. Kramer, *Cryst. Growth Des.* **2017**, *17*, 3766–3774.
[59] M. Uwaha, *J. Phys. Soc. Japan* **2004**, *73*, 2601–2603.
[60] H. Katsuno, M. Uwaha, *J. Cryst. Growth* **2014**, *401*, 59–62.
[61] M. Uwaha, *J. Phys. Soc. Japan* **2008**, *77*, 8–11.
[62] M. Uwaha, *J. Cryst. Growth* **2011**, *318*, 89–92.
[63] M. Uwaha, H. Katsuno, *J. Phys. Soc. Japan* **2009**, *78*, 2–5.
[64] M. Iggland, M. Mazzotti, *Cryst. Growth Des.* **2011**, *11*, 4611–4622.
[65] M. Iggland, R. Müller, M. Mazzotti, *Cryst. Growth Des.* **2014**, *14*, 2488–2493.
[66] J. E. Hein, B. Huynh Cao, C. Viedma, R. M. Kellogg, D. G. Blackmond, *J. Am. Chem. Soc.* **2012**, *134*, 12629–12636.
[67] D. Gherase, D. Conroy, O. K. Matar, D. G. Blackmond, *Cryst. Growth Des.* **2014**, *14*, 928–937.
[68] C. Xiouras, J. H. Ter Horst, T. Van Gerven, G. D. Stefanidis, *Cryst. Growth Des.* **2017**, *17*, 4965–4976.
[69] X. Yuchun, L. Huizhou, C. Jiayong, *Int. J. Pharm.* **2000**, *196*, 21–26.
[70] M. Sakamoto, A. Unosawa, S. Kobaru, K. Fujita, T. Mino, T. Fujita, *Chem. Commun.* **2007**, 3586.
[71] E. J. Ebbers, G. J. A. Ariaans, J. P. M. Houbiers, A. Bruggink, B. Zwanenburg, *Tetrahedron* **1997**, *53*, 9417–9476.
[72] M. Rachwalski, N. Vermue, F. P. J. T. Rutjes, *Chem. Soc. Rev.* **2013**, *42*, 9268–9282.
[73] R. Uchin, K. Suwannasang, A. E. Flood, *Chem. Eng. Technol.* **2017**, *40*, 1252–1260.
[74] W. W. Li, L. Spix, S. C. A. De Reus, H. Meekes, H. J. M. Kramer, E. Vlieg, J. H. Ter Horst, *Cryst. Growth Des.* **2016**, *16*, 5563–5570.
[75] C. Rougeot, J. E. Hein, *Org. Process Res. Dev.* **2015**, *19*, 1809–1819.
[76] A. Cohen, F. Schutze, S. Charbit, S. Bernad, C. Tauvel, M.-N. Petit, G. Coquerel, *Conglomerates of Tenatoprazole Potassium Salts*, **2007**, WO2008081104.
[77] M. J. Eicke, G. Levilain, A. Seidel-Morgenstern, *Cryst. Growth Des.* **2013**, *13*, 1638–1648.
[78] K. Galan, M. J. Eicke, M. P. Elsner, H. Lorenz, A. Seidel-Morgenstern, *Cryst. Growth Des.* **2015**, *15*, 1808–1818.
[79] R. Oketani, M. Hoquante, C. Brandel, P. Cardinael, G. Coquerel, *Cryst. Growth Des.* **2018**, *18*, 6417–6420.
[80] A. H. J. Engwerda, P. van Schayik, H. Jagtenberg, H. Meekes, F. P. J. T. Rutjes, E. Vlieg, *Chem. - A Eur. J.* **2018**, *24*, 2863–2867.
[81] M. Inagaki, J. Hiratake, T. Nishioka, J. Oda, *J. Org. Chem.* **1992**, *57*, 5643–5649.
[82] M. Smrcina, J. Polakova, S. Vyskocil, P. Kocovsky, *J. Org. Chem.* **1993**, *58*, 4534–4538.
[83] M. Pabel, A. C. Willis, S. B. Wild, *Inorg. Chem.* **1996**, *35*, 1244–1249.
[84] A. Bader, M. Pabel, A. C. Willis, S. B. Wild, *Inorg. Chem.* **1996**, *35*, 3874–3877.
[85] K. Yamada, R. Ishii, H. Nakagawa, H. Kawazura, *Tetrahedron: Asymmetry* **1996**, *7*, 737–746.
[86] D. C. R. Hockless, P. A. Gugger, P.-H. Leung, R. C. Mayadunne, M. Pabel, S. Bruce Wild, *Tetrahedron* **1997**, *53*, 4083–4094.
[87] L. Czollner, W. Frantsits, B. Küenburg, U. Hedenig, J. Fröhlich, U. Jordis, *Tetrahedron Lett.* **1998**, *39*, 2087–2088.
[88] C. A. Maryanoff, L. Scott, R. D. Shah, F. J. Villani Jr, *Tetrahedron: Asymmetry* **1998**, *9*, 3247–3250.
[89] M. Kita, K. Yamanari, *J. Chem. Soc. Dalt. Trans.* **1999**, 1221–1226.
[90] K. Yamanari, R. Ito, S. Yamamoto, A. Fuyuhiro, *Chem. Commun.* **2001**, 1414–1415.
[91] K. Yamanari, R. Ito, S. Yamamoto, T. Konno, A. Fuyuhiro, M. Kobayashi, R. Arakawa, *Dalt. Trans.* **2003**, 380–386.
[92] K. Tsubaki, M. Miura, H. Morikawa, H. Tanaka, T. Kawabata, T. Furuta, K. Tanaka, K. Fuji, *J. Am. Chem. Soc.* **2003**, *125*, 16200–16201.
[93] G. Solladié, O. Lohse, *Tetrahedron: Asymmetry* **1993**, *4*, 1547–1552.
[94] R. G. Kostyanovsky, V. R. Kostyanovsky, G. K. Kadorkina, K. A. Lyssenko, *Mendeleev Commun.* **2003**, *13*, 111–113.
[95] P. Biscarini, M. Benedetti, F. Ferranti, R. Kuroda, E. Foresti, P. Sabatino, *Chirality* **2004**, *16*, 251–262.
[96] S. Chandrasekhar, D. Chopra, T. N. Guru Row, R. Hota, T. Kanai, *J. Mol. Struct.* **2005**, *738*, 113–116.
[97] S. Chandrasekhar, S. K. Gorla, *Tetrahedron: Asymmetry* **2006**, *17*, 2247–2251.

[98] P. Biscarini, M. Benedetti, R. Kuroda, F. Ferranti, *Eur. J. Inorg. Chem.* **2006**, *2006*, 3167–3176.
[99] S. Chandrasekhar, *Chirality* **2008**, *20*, 84–95.
[100] F. Faigl, B. Mátravölgyi, T. Holczbauer, M. Czugler, J. Madarász, *Tetrahedron: Asymmetry* **2011**, *22*, 1879–1884.
[101] R. Siedlecka, *Tetrahedron* **2013**, *69*, 6331–6363.
[102] V. A. Soloshonok, V. P. Kukhar, S. V. Galushko, N. Y. Svistunova, D. V Avilov, N. A. Kuz'mina, N. I. Raevski, Y. T. Struchkov, A. P. Pysarevsky, Y. N. Belokon, *J. Chem. Soc., Perkin Trans. 1* **1993**, 3143–3155.
[103] P. Biscarini, R. Franca, R. Kuroda, *Inorg. Chem.* **1995**, *34*, 4618–4626.
[104] R. Noyori, M. Tokunaga, M. Kitamura, *Bull. Chem. Soc. Jpn.* **1995**, *68*, 36–55.
[105] E. Vedejs, S. C. Fields, S. Lin, M. R. Schrimpf, *J. Org. Chem.* **1995**, *60*, 3028–3034.
[106] M. Pabel, A. C. Willis, S. B. Wild, *Tetrahedron: Asymmetry* **1995**, *6*, 2369–2374.
[107] H. van der Deen, A. D. Cuiper, R. P. Hof, A. van Oeveren, B. L. Feringa, R. M. Kellogg, *J. Am. Chem. Soc.* **1996**, *118*, 3801–3803.
[108] M. Pabel, A. C. Willis, S. B. Wild, *Inorg. Chem.* **1996**, *35*, 1244–1249.
[109] S. Gonella, G. Levilain, G. Coquerel, *J. Therm. Anal. Calorim.* **2011**, *103*, 125–129.
[110] C. Brandel, G. Gbabode, Y. Cartigny, C. Martin, G. Gouhier, S. Petit, G. Coquerel, *Chem. Mater.* **2014**, *26*, 4151–4162.
[111] S. R. Laplante, L. D. Fader, K. R. Fandrick, D. R. Fandrick, O. Hucke, R. Kemper, S. P. F. Miller, P. J. Edwards, *J. Med. Chem.* **2011**, *54*, 7005–7022.
[112] G. Coquerel, in *Polymorph. Pharm. Ind.*, Wiley-VCH Verlag GmbH & Co. KGaA, Weinheim, Germany, **2018**, pp. 91–132.
[113] C. Brandel, Y. Cartigny, G. Coquerel, J. H. ter Horst, S. Petit, *Chem. - A Eur. J.* **2016**, *22*, 16103–16112.
[114] E. Temmel, M. J. Eicke, F. Cascella, A. Seidel-Morgenstern, H. Lorenz, *Cryst. Growth Des.* **2019**, *19*, acs.cgd.8b01660.
[115] C. Brandel, Y. Amharar, J. M. Rollinger, U. J. Griesser, Y. Cartigny, S. Petit, G. Coquerel, *Mol. Pharm.* **2013**, *10*, 3850–3861.
[116] M. Sakamoto, A. Unosawa, S. Kobaru, A. Saito, T. Mino, T. Fujita, *Angew. Chemie - Int. Ed.* **2005**, *44*, 5523–5526.
[117] G. Coquerel, in *Adv. Org. Cryst. Chem.* (Eds.: R. Tamura, M. Miyata), Springer Japan, Tokyo, **2015**, pp. 393–420.
[118] G. Coquerel, *J. Pharm. Pharmacol.* **2015**, *67*, 869–878.
[119] S. Gonella, G. Levilain, G. Coquerel, *J. Therm. Anal. Calorim.* **2011**, *103*, 125–129.
[120] G. Coquerel, in *Polymorph. Pharm. Ind.*, Wiley-VCH Verlag GmbH & Co. KGaA, Weinheim, Germany, **2018**, pp. 91–132.
[121] W. L. Noorduin, B. Kaptein, H. Meekes, W. J. P. Van Enckevort, R. M. Kellogg, E. Vlieg, *Angew. Chemie - Int. Ed.* **2009**, *48*, 4581–4583.
[122] G. Coquerel, *Chem. Soc. Rev.* **2014**, *43*, 2286–300.
[123] J. W. Mullin, *Crystallization*, Butterworth-Heinemann, **2001**.
[124] F. Breveglieri, M. Mazzotti, *Cryst. Growth Des.* **2019**, *19*, 3551–3558.

CV, List of publications, and Communications in international meetings

NAME	**Ryusei OKETANI**
ELECTRIC DIRECTORY	*E-mail:* ryusei.oketani@etu.univ-rouen.fr / ryuseioketani@gmail.com *Website:* http://labusers.net/~oketani/ *ORCID:* https://orcid.org/0000-0001-7860-2456
ADDRESS	Laboratoire Sciences et Méthodes Séparatives Université de Rouen Normandie Place Emile Blondel 76821 Mont Saint Aignan Cedex FRANCE

EDUCATION

Ph.D., Chemistry (To be defended on 6th December 2019)
Université de Rouen Normandie, Mont Saint Aignan, France
Dissertation Title: Practical aspects on how to deracemize atropisomers by means of crystallization

M.A., Human and Environmental Studies (2016)
Kyoto University, Kyoto, Japan
Thesis title: Theoretical and experimental study on storing energy gas into organic molecular crystals

B.Eng., Chemistry (2014)
Osaka Prefecture University College of Technology, Osaka, Japan
Thesis title: Study on applying TiO_2 photocatalytic reaction to organic syntheses

OTHER EXPERIENCE

External PhD student (April – May 2019)
Merck KGaA, Darmstadt, Germany

Visiting student (October – November 2018)
Radboud Univeristy Nijmegen, Nijmegen, Netherlands

Academic guest (October 2017)
ETH Zurich, Zurich, Switzerland

Technical trainee (January 2015)
National Institute of Advanced Industrial Science and Technology (AIST), Ibaraki, Japan

Internship student (August 2012)
Sumitomo Chemical, Osaka, Japan

PUBLICATIONS

Journal Articles

[6] Deracemization in a complex quaternary system with a second-order asymmetric transformation using phase diagram studies. R. Oketani, F. Marin, P. Tinnemans, M. Hoquante, A. Laurent, C. Brandel, P. Cardinael, H. Meekes, E. Vlieg, Y. Geerts, G. Coquerel, *Chem. Eur. J.*, **2019**, *25*, 13890-13898.

[5] Resolution of an atropoisomeric naphthamide by second-order asymmetric transformation: A highly productive technique. R. Oketani, M. Hoquante, C. Brandel, P. Cardinael, G. Coquerel, *Org. Process Res. Dev.,* **2019**, *23*, 1197-1203.

[4] NH-form of a threonine-based Schiff base in the solid state. R. Oketani, H. Takahashi, M. Hoquante, C. Brandel, P. Cardinael, G. Coquerel, *J. Mol. Struct.*, **2019**, 1184, 36-40.

[3] Effect of Substituents on TiO_2 photocatalytic Oxidation of trans-Stilbenes. T. Miyake, Y. Hashimoto, S. Jinnai, R. Oketani, S. Higashida, *Bull. Chem. Soc. Japan*, **2019**, *92*, 55-60.

[2] Practical Role of Racemization Rates in Deracemization Kinetics and Process Productivities. R. Oketani, M. Hoquante, C. Crandel, P. Cardinael, G. Coquerel, *Cryst. Growth Des.,* **2018**, *18*, 6417-6420.

[1] Formation of Lactones by Decarboxylation of Aromatic Diacids via TiO_2-Mediated Photocatalytic Reactions in Acetonitrile Solution. R. Oketani, T. Miyake, S. Jinnai, T. Fukui, H. Tsujimoto, M. Matsumura, S. Higashida, *Chem. Lett.* **2016**, 45, 801-803.

Book Chapter

[1] Azacalixarene: an ever-growing class in the calixarene family. H. Tsue and R. Oketani, In *Advances in Organic Crystal Chemistry: Comprehensive Reviews 2015*, R.Tamura and M.Miyata (eds.), Springer, Chapter 13, 241-261.

AWARDS

[12] Chemistry of Materials Best Poster Prize, The 24th International Conference on the Chemistry of the Organic Solid State (ICCOSS XXIV 2019), June 20, 2019.

[11] Poster Prize, Symposium on Molecular Chirality 2018, May 12, 2018.

[10] Outstanding Poster Presentation Award, The 22nd International Conference on the Chemistry of the Organic Solid State (ICCOSS XXII JAPAN 2015), July 16, 2015.

[9] Best Poster Prize, The 23rd Organic Crystal Symposium, September 17, 2014.

[8] Presidential Award for Encouragement, Oaka Prefecture University College of Technology, March 18, 2014.

[7] 1st Prize in JASSO's Student of the Year 2013, The Japan Student Services Organization, December 9, 2013.

[6] Poster Prize, Japan Association for College of Technology The 19th annual meeting, August 31, 2013.

[5] Best Presentation Prize, The Society for Mathematical Sciences The 32nd annual meeting, August 27, 2013.

[4] Presidential Award for Encouragement, Osaka Prefecture University College of Technology, March 19, 2013.

[3] Best Poster Prize, Osaka Prefecture University College of Technology Area Interchange Messe, March 7, 2013.

[2] Best Poster Prize, Japan Association for College of Technology The 18th annual meeting, August 25, 2012.

[1] Chemical Society of Japan Kinki Branch Manager Prize, The 14th College of Technology Chemistry meeting, March 13, 2012.

PRESENTATION

International Conference

[10] Phase diagram study and chiral resolution of axially chiral naphthamide derivative. R. Oketani, M. Hoquante, C. Brandel, S. Clevers, F. Marin, P. Tinnemans, H. Meekes, E. Vlieg, Y. Geerts, P. Cardinael, G. Coquerel, 24th International Conference on the Chemistry of the Organic Solid State (ICCOSS XXIV 2019), New York, June 2019.

[9] Phase equilibria between atropisomers: Chirality Induced by Dissymmetric Distribution. F.X. Gendron, R. Oketani, G. Coquerel, Journées André Collet de la Chiralité (JACC 2018), Noirmoutier, September 2018.

[8] Interplay of the racemization rate and the crystal growth rate on the deracemization rate. R. Oketani, C. Brandel, P. Cardinael, G. Coquerel, The 25th Bremen International Workshop on Industrial Crystallization (BIWIC2018), Rouen, September 2018.

[7] The role of racemization and crystal growth kinetics on deracemization rate of naphthamide compound using temperature cycling. R. Oketani, C. Brandel, P. Cardinael, G. Coquerel, 13th International Workshop of the Crystal Growth of Organic Material (CGOM13), Seoul, August 2018.

[6] Complex behaviors in a system composed of two couples of atropisomers: heterogeneous equilibria, crystallography and deracemization. G. Coquerel, R. Oketani, F.X. Gendron, R. Kuroda, 13th International Workshop of the Crystal Growth of Organic Material (CGOM13), Seoul, August 2018.

[5] Crystal structure and gas adsorption behavior of magnesium porphyrin with open coordination sites. R. Oketani, H. Takahashi, R. Tamura, H. Tsue, Pacifichem 2015, Honolulu, December 2015.

[4] X-ray Crystallographic Analysis of CO_2 Adsorption State in Seemingly Nonporous Crystal of *N,C*-Proteced Methionylalanine. R. Oketani, Y. Mori, K. Sasaki, H. Takahashi, R. Tamura, H. Tsue, 22nd International Conference on the Chemistry of the Organic Solid State (ICCOSS XXII JAPAN 2015), Niigata, July 2015.

[3] Formation of Lactones from Aromatic Diacid Compounds in Acetonitrile Solution by TiO_2-Photocatalytic Reactions. R. Oketani, S. Higashida, M. Matsumura, The Seventh Tokyo Conference on Advanced Catalytic Science and Technology (TOCAT7), Kyoto, June 2014.

[2] Effects of Additive Agents on Oxidative Cleavage Reaction of trans-Stilbene using TiO_2 Photocatalyst in Acetonitrile Solution. T. Miyake, R. Oketani, S. Higashida, M. Matsumura, The 17th SANKEN International Symposium, Osaka, January 2014.

[1] Demonstration display of the railroad model vehicle which carried a fuel cell system. R. Oketani, T. Uemoto, F. Nagano, M. Yamauchi, K. Sugiura, SEMICON JAPAN2013 “The KOSEN@SEMICON”, Chiba, December 2013.

Abstract

Chiral separation techniques are important for enabling studies relating to the biological functions and activities of chiral molecules. In this thesis, chiral separations by deracemization, an approach that combines racemization with crystallization, have been studied from the practical and theoretical viewpoints using atropisomeric naphthamide.

In Chapter 2, we studied the first experimental proof of the impact of racemization kinetics on global temperature cycle induced deracemization (TCID) kinetics as well as on process productivity. The racemization kinetics are linearly related to the global TCID kinetics, and the process productivity was related not only to the racemization kinetics but also to the solubility of the compound. In Chapter 3, we performed a comparison study of process productivities of TCID and second-order asymmetric transformation (SOAT). We demonstrated that the process productivity of TCID is independent of the scale of the system. Then, we found that SOAT is a productive process, while TCID gives highly enantiopure products. In Chapter 4, a problematic case of the deracemization of a single compound forming multiple solid phases was demonstrated using a phase diagram study. Although racemization adds complexity to the phase diagram, we sought to show the construction of a phase diagram for racemizable compounds and how the diagram enabling deracemization.

Résumé

Les techniques de séparation chirale sont importantes pour permettre des études relatives de l'activité biologique des molécules chirales. Dans cette thèse, la séparation chirale des atropisomères de la naphthamide par déracémisation, une approche combinant la racémisation avec la cristallisation, a été étudiée du point de vue pratique et théorique. Dans le chapitre 2, nous avons démontré pour la première fois l'impact de la cinétique de racémisation sur la cinétique de déracémisation induite par des cycles de température (TCID) ainsi que sur la productivité du processus. La cinétique de racémisation est liée linéairement à la cinétique globale TCID, et la productivité du procédé est liée non seulement à la cinétique de racémisation mais également à la solubilité du composé dans le solvant choisi. Dans le chapitre 3, nous avons comparés les productivités des processus de TCID et de transformation asymétrique de second ordre (SOAT). Nous avons démontré que la productivité des processus de TCID est indépendante de l'échelle du système. Ensuite, nous avons montré que SOAT est un processus permettant d'obtenir la meilleure productivité, tandis que le TCID permet d'obtenir des produits hautement énantiopurs. Dans le chapitre 4, un cas problématique de déracémisation d'un composé formant plusieurs phases solides a été réalisée à l'aide d'une étude de diagramme de phases. Bien que la racémisation ajoute de la complexité au diagramme de phase, nous avons montré la construction d'un diagramme de phase pour les composés racémisables permet de trouver les conditions permettant de mener à bien le procédé de déracémisation.